LEVEL II

INTELLIGENT TRACKING TECHNIQUES

FOURTH QUARTERLY REPORT

for

September 30, 1979

CONTRACT: DAAK 70-78-C-0167

Presented to

Night Vision and Electro-Optics Laboratory
Fort Belvoir, Virginia 22060

Submitted by

Westinghouse Electric Corporation
Systems Development Division
Baltimore, Maryland 21203

INTELLIGENT TRACKING TECHNIQUES

FOURTH QUARTERLY REPORT

for

September 30, 1979

CONTRACT: DAAK 70-78-C-0167

Presented to

Night Vision and Electro-Optics Laboratory
Fort Belvoir, Virginia 22060

Submitted by

Westinghouse Electric Corporation
Systems Development Division
Baltimore, Maryland 21203

SECURITY CLASSIFICATION OF THIS PAGE (When Data Entered)

REPORT DOCUMENTATION PAGE

READ INSTRUCTIONS BEFORE COMPLETING FORM

1. REPORT NUMBER	2. GOVT ACCESSION NO. AD-A086 752 / AD82 183.
3. RECIPIENT'S CATALOG NUMBER	
4. TITLE (and Subtitle) (6) Intelligent Tracking Techniques / ~~Fourth Quarterly Report~~	5. TYPE OF REPORT & PERIOD COVERED Fourth Quarterly Report July 1, 1979 - Sept. 30, 1979
	6. PERFORMING ORG. REPORT NUMBER
7. AUTHOR(s) T.J. Willett, et.al.	8. CONTRACT OR GRANT NUMBER(s) (15) DAAK 70-78-C-0167
9. PERFORMING ORGANIZATION NAME AND ADDRESS Systems Development Division ✓ Westinghouse Electric Corporation Baltimore, Maryland 21203	10. PROGRAM ELEMENT, PROJECT, TASK AREA & WORK UNIT NUMBERS (12) 74
11. CONTROLLING OFFICE NAME AND ADDRESS U.S. Army Night Vision and Electro-Optics Laboratory Fort Belvoir, Virginia 22060	12. REPORT DATE Sept. 30, 1979
	13. NUMBER OF PAGES 63
14. MONITORING AGENCY NAME & ADDRESS (if different from Controlling Office) (11) Sep 79	15. SECURITY CLASS. (of this report) Unclassified
	15a. DECLASSIFICATION/DOWNGRADING SCHEDULE

16. DISTRIBUTION STATEMENT (of this Report)

Distribution Unlimited

DISTRIBUTION STATEMENT A
Approved for public release;
Distribution Unlimited

17. DISTRIBUTION STATEMENT (of the abstract entered in Block 20, if different from Report)

(1) Quarterly Rept. no. 4, 1 Jul-30 Sep 79,

18. SUPPLEMENTARY NOTES

(10) Thom. J. Willett

19. KEY WORDS (Continue on reverse side if necessary and identify by block number)

Automatic Target Cueing	TV Sensor
Target Recognition	Digital Image Processing
Target Tracking	Correlation Tracking
FLIR Sensor	Target Homing

20. ABSTRACT (Continue on reverse side if necessary and identify by block number)

This is the Fourth Quarterly Report under a contract to investigate the design, test, and implementation of a set of algorithms to perform intelligent tracking and intelligent target homing on FLIR and TV imagery. The intelligent tracker will monitor the entire field of view, detect and classify targets, perform multiple target tracking and predict changes in target signature prior to the target's entry into an obscuration. The intelligent tracking and homing system will also perform target prioritization and critical aimpoint selection.

DD FORM 1 JAN 73 1473 EDITION OF 1 NOV 65 IS OBSOLETE

405 897

SECURITY CLASSIFICATION OF THIS PAGE (When Data Entered)

A system concept was developed for intelligent homing and aimpoint selection. The problem was divided into long range homing and aimpoint selection and close-in homing and aimpoint selection. Sets of 875-line FLIR imagery were extracted from the NV&EOL data base and examples were presented for both categories. The subjects of close-in homing and aimpoint selection were further divided into close-in segmentation, close-in target tracking, and tracking during the transition from long range to close-in.

TABLE OF CONTENTS

	Page
INTRODUCTION	1
1.0 SYSTEM CONCEPT	1-1
1.1 Target Acquisition and Handover	1-3
1.2 Multiple Target Tracking	1-3
1.3 Target Signature Prediction	1-4
1.4 Reacquisition	1-5
1.5 Aimpoint Selection	1-5
2.0 WEAPON ANALYSIS	2-1
2.1 Mission Requirements	2-2
2.2 Design Constraints	2-4
2.3 System Design Requirements	2-6
2.4 Body Fixed vs Gimbaled Sensor	2-7
3.0 INTELLIGENT HOMING	3-1
3.1 Related Work	3-1
3.2 Extending Ground Coverage	3-2
3.3 Aimpoint Selection	3-3
3.3.1 exterior based aimpoint selection	3-4
3.3.2 interior based aimpoint selection	3-8
4.0 PRELIMINARY RESULTS	4-1
4.1 Long Range Aimpoint Selection	4-1
4.2 Close-in Homing and Aimpoint Selection	4-12
4.2.1 close-in segmentation	4-12
4.2.2 close-in target tracking	4-20
4.2.3 tracking during transition	4-34

INTRODUCTION

Under contract to the Army's Night Vision and Electro-Optics Laboratory, Westinghouse has been investigating the design, test, and implementation of a set of algorithms to perform intelligent tracking and intelligent target homing on FLIR and TV imagery. Research has been initiated for the development of an intelligent target tracking and homing system which will combine target cueing, target signature prediction, and target tracking techniques for near zero break lock performance. The intelligent tracker will monitor the entire field of view, detect and classify targets, perform multiple target tracking, and predict changes in target signature prior to the target's entry into an obscuration. The intelligent tracking and homing system will also perform target prioritization and critical aimpoint selection. Through the use of VLSI/VHSI techniques, the intelligent tracker (with inherent target cuer) can be applied to the fully autonomous munition.

During the fourth quarter, several meetings and a number of phone conversations took place between Westinghouse personnel and Cpt. Reischer of NV&EOL. A system concept was developed for intelligent homing and aimpoint selection. The problem was divided into long range homing and aimpoint selection and close-in homing and aimpoint selection. Sets of 875 line FLIR imagery were extracted from the NV&EOL data base and examples were presented for both categories. The subjects of close-in homing and aimpoint selection were further divided into close-in segmentation, close-in target tracking and tracking during the transition from long range to close-in.

Westinghouse personnel participating in this effort include Thomas Willett, Program Manager, Dr. John Romanski, John Shipley, Leo Kossa, Bill Pleasance, and Richard Kroupa. Program review and consultation is provided by Drs. Glenn Tisdale and Azriel Rosenfeld.

1.0 SYSTEM CONCEPT

The purpose of this section is to describe the preliminary intelligent tracker concept that has evolved during the course of this work. The desired intelligent tracker functions are:

1. acquisition and track initiation - detect, locate, classify and prioritize targets automatically and handoff to the internal tracker (the intellignet tracker concept is assumed to include both acquisition and tracking);
2. handle multiple targets - track a number of targets in a scene simultaneously;
3. target signature prediction - predict or anticipate target obscuration and how the target signature will change as a result of the obscuration;
4. reacquisition - reacquire a target at the earliest opportunity following track break lock, including departure from the field of view;
5. aimpoint selection - determine the critical aimpoint of a target which may be an interior point within its silhouette.

A video timing diagram is shown in Figure 1-1. Figure 1-2 shows how an image appears in the frame store device. A block diagram of the system concept is shown in Figure 1-3.

The heavy vertical lines in Figure 1-1 represent the cued frames and the lighter vertical lines are the tracked frames. Frame 1 is a cueing frame, and frames 2, 3, 4, and 5 are tracking frames and then the cycle repeats. Frame 6 is a cueing frame, and frames 7, 8, 9, and 10 are tracking frames. Thus the complex target cueing function is performed at 0.2 the rate of the simpler tracking function. Figure 1-2 represents the image in the frame store which is divided into five horizontal and addressable strips. This is done so that, instead of waiting for the entire frame to be cued

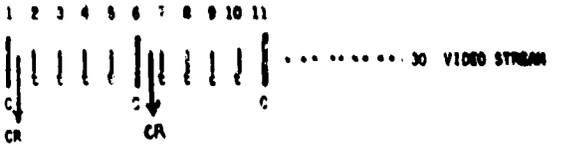

Figure 1-1. Timing Diagram

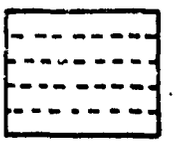

Figure 1-2. Image In Frame Store RAM

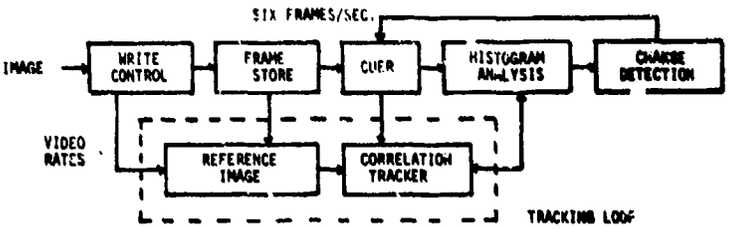

Figure 1-3. System Block Diagram

before handover to a tracker, targets can be handed over more rapidly. The reduction in handover lag increases the confidence that both cuer and tracker are working on the same target, and reduces the size of the track window. The frame store RAM is organized into five independently addressable strips to aid in sending the gray levels surrounding the target to the tracker for a reference image and to decrease the access time. It should be pointed out that the five tracked frames per cued frame and five strips for frame storage are approximate numbers serving as a straw man concept. The point of this discussion is that the cuer results, labelled CR, in Figure 1-1 can be obtained between the first and second frames instead of the fifth and sixth frames in the video stream.

Referring to Figure 1-3, we describe the intelligent tracker functions previously listed:

1.1 TARGET ACQUISITION AND HANDOVER

A horizontal strip of a frame is snatched in real time and placed in a frame store. The cuer processes the strip and detects and classifies all targets. That part of the frame store holding each target and its surrounding gray scale window is sent to the tracker as a reference image. The tracker converts this to a binary reference image and now tracks this target from the video stream until the next cued frame. The cuer tells the tracker where the target is within the frame so the tracker can tell the write control when to write the next target window (now from the video stream) and subsequent windows into its reference image.

1.2 MULTIPLE TARGET TRACKING

There is a reference image RAM reserved for each target. Only one tracker is required, since it is fast enough to be multiplexed among targets. The tracker is a bandpass binary correlation tracker in this preliminary de-

sign and the bandpass is adjusted at the cueing rate by the cuer. Additionally, the tracker forms a smoothed track for each target in second order difference equations (to interface with the rate loop in the sensor gimbal). This allows reacquisition of a target which has left the field of view but can be brought back into view by moving the sensor along the image centered target track.

At this point one can picture simultaneous multitarget cueing and tracking. The cued targets have been classified and are ordered in an internal table in terms of priority. The priority precedence has been determined before the mission and loaded in the cuer.

1.3 TARGET SIGNATURE PREDICTION

To predict obscurations, a histogram of the background ahead of the target is analyzed. The track window errors, which are used to form the smoothed track for reacquisition, are also used to determine the position of the histogram window in front of the target. From the histogram, we can compare the gray levels ahead of the target with those of the target. If the same gray levels are present in both, a clean target segmentation is unlikely. The track point position is adjusted within the track reference window so that the tracker is using that portion of the target which will be obscured last (e.g. the rear of a target passing behind some low lying shrubs). The background histogram is also analyzed for a polarity reversal between the target and the background. An example of this is a case where the target is moving from a dark background into one lighter than itself and hence becomes a dark target against a light background. Under this condition, the new background is segmented and binary change detection at the background level is used along with direct segmentation to detect the target. Having found the front edge of the target, the track point in the reference is adjusted to the front or emerging edge.

1.4 REACQUISITION

The reacquisition function comes into play when track breaklock occurs. It is handled by a combination of cueing, histogram analysis, and change detection. A difficult problem here is the reappearance of a target which is partially obscured. Segmentation of the entire shape is not possible which prevents automatic target recognition. In this case scene change detection provides one of the few cues of target reemergence. histogram analysis of any changed areas found adds useful information because, in some cases, the target histogram will exhibit a peakedness not found in a background object such as a woods clearing. That is, the histogram will resemble a Gaussian rather than a Uniform Distribution. Otherwise, the clearing may be mistaken for a partially occluded target.

1.5 AIMPOINT SELECTION

This is the topic for this quarterly and the next one; it involves performing aimpoint selection on both the exterior and interior of a target.

2.0 WEAPON ANALYSIS

To properly attack the intelligent tracking and homing problem, it is necessary to consider the entire weapon system including the sensor. The design of an efficient weapon system can be aided by use of operations analysis and system design. Operations analysis examines the existing and projected personnel and material to estimate the cost of the business of war. Key determinations are the initial and recurring costs of maintaining weapons and troops in readiness, and the exchange rates expected between clashing units of force. A war of attrition is anticipated which will involve quantities of material large enough for statistical averages to be meaningful. Operations analysis will quantify the need for a new weapon capability by specifying such things as the maximum cost per round of munition as a function of the probability of kill per round. System design starts with the weapon system requirements thus provided and produces specifications for subsystems to efficiently meet the requirements. The subsystems are dealt with in terms of parameters which primarily determine performance and cost. The primary objective, the most efficient system design, is obtained by making tradeoffs between subsystems.

It is not within the scope of this contract to design a weapon system. We are limited to consideration of the narrow issue of analyzing the intelligent tracking and homing problem within the confines of an existing weapon system, e.g. the Copperhead Missile. The following paragraphs of this section list parameters that affect mission success, including the assumptions used in obtaining them; describe the Copperhead weapon; present an example to indicate sensor requirements; and analyze the advantages of a body fixed system and a gimballed sensor system.

2.1 MISSION REQUIREMENTS

Some aspects of the operation of an intelligent tracking and homing system, which impacts both effectiveness and cost, are outlined here. These include footprint, target discrimination, impact CEP, and countermeasures.

Footprint - The largest dimension to which the footprint can be related is the kill range of the projectile. A maneuver capability this large would obviate the need to aim the projectile at launch. Since the aiming capability already exists, a footprint as large as the range will not be considered further.

The next largest relevant dimension is the uncertainty in location of the targets. In an assumed five minute lag between reconnaissance and strike, a tank can travel a maximum of 4 km, assuming a top speed of 30 miles/hour. A group of tanks might achieve a maximum travel of 2 km in five minutes while making acceptable average progress toward their objective. Therefore, strikes against isolated groups of targets might benefit by a footprint 2 km wide. However, an important application of the weapon is defense against a massive attack. In this case, the spacing between groups might be only a fraction of a kilometer, and the requirement to intercept a particular group of targets does hold.

A still lower relevant dimension is the 0.3 km CEP ballistic dispersion. A 0.5 km wide footprint would have a 0.5 probability of hitting a single target at the ballistic aimpoint. The lowest dimensions significant to the footprint are the approxiamtely 0.4 km group size and 0.1 km spacing of targets within a group.[1] Because of this spacing, a footprint somewhat smaller than 0.6 km would probably still retain a high probability of reaching a target.

There might be justification for a footprint as low as 0.1 km spacing, even though this would reduce the probability of reaching a target. A maneuver footprint considerably smaller than the ballistic dispersion would serve to disperse multiple rounds over multiple targets. If the cost of this limited capability is sufficiently low, it would compensate for the greater number of rounds required per kill. It is assumed that a footprint of 0.6 km is effective.

1. Unpublished Westinghouse work in support of F-16, July 1979 by W.E. Pleasance.

Target Discrimination - In order to home on a specific target, it must be distinguished from other objects in the field of view. The effectiveness of the weapon will depend on the accuracy of the discrimination function. Several levels of discrimination will be considered.

1. Object detection - If the weapon is able to avoid open areas and hit an object about the size of a target, performance might be sufficiently effective provided the FOV is initialized correctly and provided few non-target objects of similar size, such as trees, are in the area.

2. Discrimination between man-made and natural objects - if a high probability of distinguishing man-made objects is provided by detecting straight edges and right angles,for instance, effectiveness would be increased.

3. Discrimination of vehicles vs other man-made objects - detection of wheels or motion would contribute to this.

4. Discrimination between tanks and other vehicles - discrimination of the highest value targets would allow the most expensive weapon to be used.

5. Discrimination between active and destroyed vehicles - this capability would allow the weapon to avoid a target already killed.

6. Target clusters - effectiveness against merged targets might also be achieved by the following means. Multiple hits on the same target could be avoided if each weapon is assigned an individual target within the field of view and/or within a group of targets. The assignment could be made by labelling the targets relative to a set of two-dimensional coordinates, such as sensor azimuth and elevation or the major and minor axis of the target distribution. This would not be as effective as discrimination against destroyed targets.

Impact CEP- The circular error probability of impact relative to a desired aimpoint has a maximum limit of approximately 1.5 m which is necessary in order to attain a sufficiently high probability of kill of armored vehicles by available warheads. A CEP less than this, but greater than about 0.5 m might permit use of a less destructive warhead and/or shallower impact angles. A reduction of CEP below this lower value is not likely to increase effectiveness much unless a value on the order to centimeters should be attained, because such things as viewing ports and gun muzzle might be more vulnerable. A 1.0 m CEP is assumed necessary for the warhead.

Countermeasures - The weapon cost must be low relative not only to the target but also to any equipment which reduces its effectiveness. Effectiveness must be maintained in spite of enemy tactics encountered during an attack. One tactic which would counter an IR guided weapon would be to launch an attack in low visibility weather. An intermediate condition would be a low cloud ceiling with good visibility. A shallow trajectory would counter this restriction to operation, but would probably require more comprehensive image processing.

2.2 DESIGN CONSTRAINTS

In the absence of complete information about existing guided missiles and tanks, the following list of parameters, (some of which represent Copperhead) was assembled from unclassified sources and assumptions based on requirements.

WEAPON

Length	137 cm
Diameter	15.5 cm
Weight	64 kg
Range (ballistic)	3 - 20 km
(gliding)	8 - 20 km
Speed	500 m/sec.
Ballistic Dispersion	300 m
Maximum Maneuver	3 g
Roll Rate	6 - 18 revs/sec.
Autopilot Time Constant	0.1/sec.
Guidance	proportional
Gimbal Limits	±45 deg
Maximum Aperture	12 cm
Warhead Capability	top and side armor
Maximum Impact Angle	±45 deg

TANK

Length	6.6 m
Width	3.3 m
Height	2.4 m
Maximum Speed	49 km/hour
Equipment	Smoke Generator
	Removable Snorkle
	Night Vision
Deployment	10 per 0.3 to 0.5 km column

In addition, it is assumed that a 1.0 m CEP of impact relative to an aimpoint is required for acceptable effectiveness.

2.3 SYSTEM DESIGN CONSIDERATIONS

A complete system design for a new guided weapon would be most efficient if all subsystems were considered. However, in the present study we will consider only the design of the sensor-tracker and assume that the airframe, warhead, and autopilot are specified. The Copperhead projectile will be used for this purpose. An objective of the study will be to minimize the demand on the sensor-tracker by using the capabilities of the remaining subsystems to the greatest extent possible. In particular, the use of the maximum maneuver capability of the airframe will allow the shortest possible detection range and hence the lowest sensor resolution. The following example indicates the considerations involved. A possible geometrical relationship in a target area is shown in Figure 2-1.

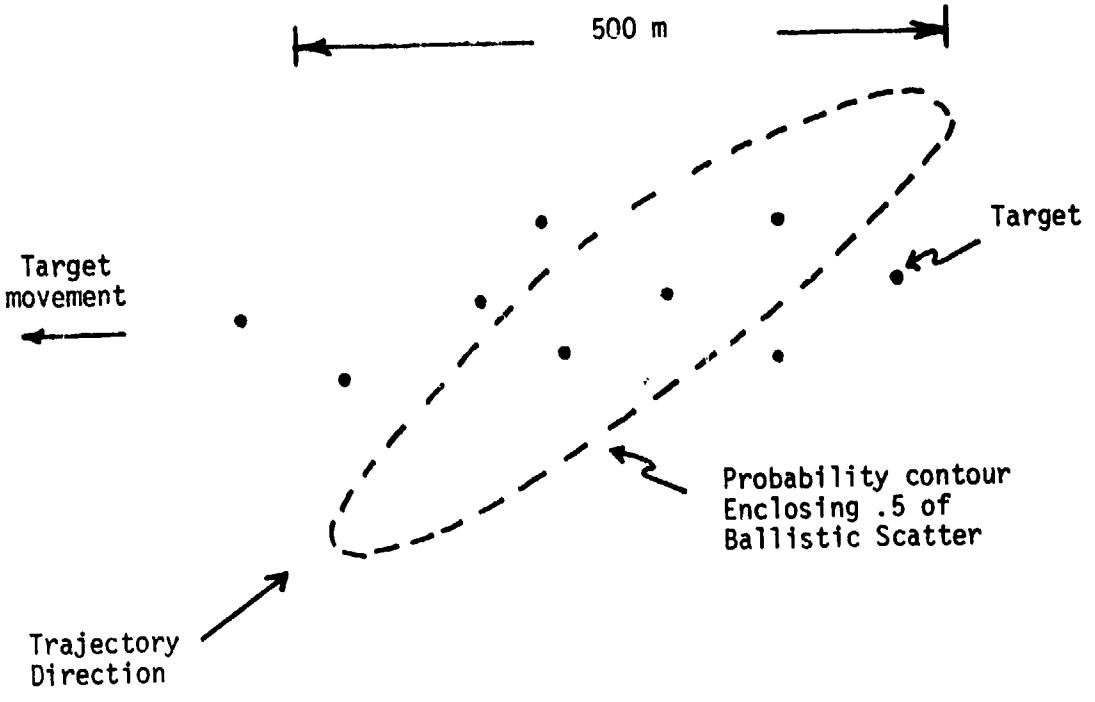

Figure 2-1. Assumed Target Area

A performance parameter of major importance which must be assumed at this time is the size of the maneuver footprint required of the weapon. A maneuver radius equal to 300 m ballistic CEP will be assumed. For the expected target

spacing, this radius would provide a high probability that each projectile would reach a target if the ballistic aimpoint is the center of a cluster of targets. For a 8.5 km minimum turn radius and 0.5 km of trajectory required for guidance settling, a turn must be initiated as far as 2.7 km from the target. At this range, detection of a target must have occurred. If six resolution elements are required across a 2.4 m target to achieve detection, an angular resolution of 2.4/6(2700) = 0.15 mrad. is required. The necessary optical aperture is at least 9.0 cm at 10μ. The angle subtended by the 300m maneuver radius at the turn initiation point is 7 degrees. This means that a field of view of 0.24 radians would be required to encompass the maneuver footprint. With one pixel per resolution element, an image of 610 pixels on a side would be required.

To be consistent with the maximum maneuver assumption of 3 g's (page 2-5), we stipulate that the platform must turn towards detected targets at a range of 2.7 km. Target classification and prioritization, requiring 10 lines on the target, occurs at a range of 1.6 km. These maximum maneuver relationships are summarized in Figure 2-2. This estimate assumes a negligible blind range. This is reasonable since the target will fill the field of view at a range of about 27m.

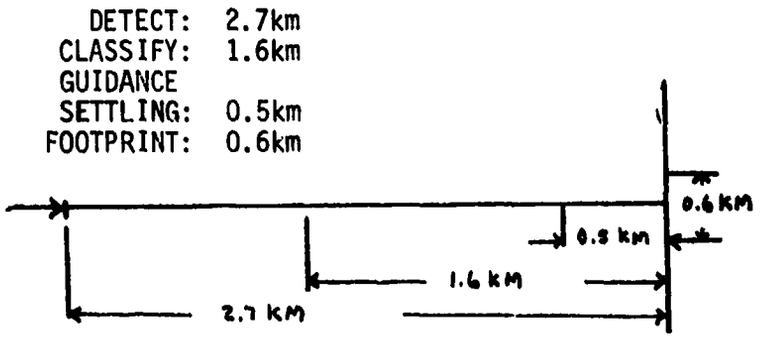

Figure 2-2. Homing Events vs. Distance

2.4 BODY FIXED VS GIMBALED SENSOR

Although the simplicity of a body fixed sensor might contribute more to reduced cost and increased reliability than a gimbaled sensor for a small homing weapon, the particular homing technique is a major consideration. Figure 2-3 shows three possible implementations of homing guidance. They have in common a simplicity of control signal processing which rotates the missile body until a directly measured sensor quantity is nulled. The first implementation, pursuit, nulls the angle between the measured target position, within the field of view, and the missile longitudinal axis. The second, closing, nulls the angle between the missile velocity vector and the measured target position within the field of view (line of sight). The third, proportional, nulls the line of sight (LOS) angle rate relative to an inertial, non-rotating, reference. The angle between the measured target position, within the field of view, and some reference is called the line of sight (LOS) angle. In the pursuit case, the LOS angle is relative to the missile longitudinal axis; in the closing case, the LOS angle is relative to the missile velocity vector; in the proportional case, the LOS angle is relative to an inertial reference. The first two systems are position controllers, while the third is a rate controller.

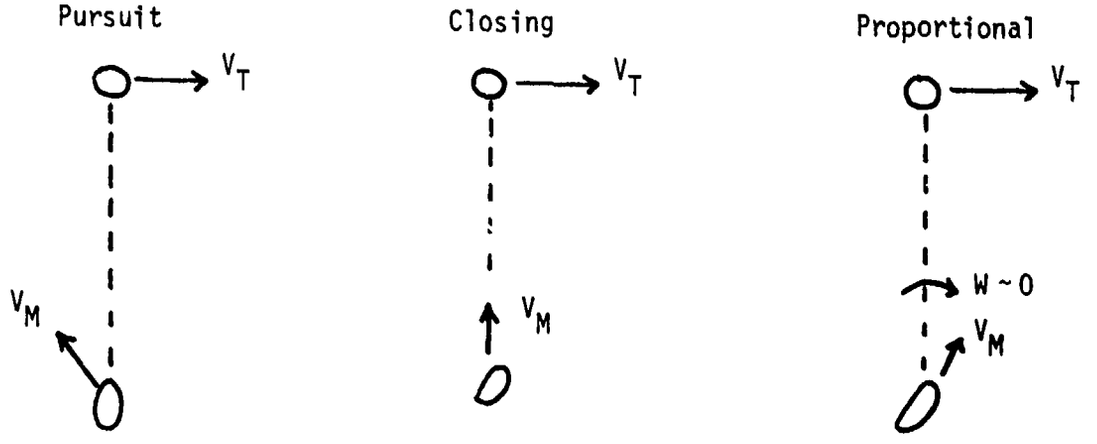

Figure 2-3. Homing Strategies

Pursuit guidance, shown at the left of Figure 2-3, is the simplest; the output of the sensor is connected to the control loop. However, a problem arises with pursuit guidance; as the body is rotated to null the LOS angle relative to the longitudinal axis, the missile velocity vector is lagging behind. Figure 2-3 shows the missile pointed at the target but the missile is still moving along its velocity vector, V_M. In general, changes in the velocity vector will lag changes in the line of sight angle. Acceptable miss distance is possible only with low target crossing velocities and practically no acceleration. Even with a fixed target, unintended missile acceleration must be minimized. Gravitational acceleration might be avoided by a terminal trajectory that is very close to vertical. Otherwise, it must be compensated by reference to a vertical gyro for instance. Another source of acceleration which might limit accuracy is the gradient of wind speed with altitude. The targets of interest are expected to have accelerations of about 0.2g when following curved roads. Therefore, a more effective control must be implemented.

The second of the three guidance methods appears most effective for a fixed sensor. Although lacking a standard designation, it is referred to as closing guidance for the sake of discussion. This is mechanized in some bomb laser kits. The velocity reference is obtained by putting the sensor in a wind vane pod ahead of the bomb. If such a pivoted device is not practical for a projectile, alternate techniques could be used to provide the velocity reference. Closing guidance is less demanding on the imaging sensor for a fixed sensor configuration than proportional guidance. Closing guidance is more demanding for a fixed sensor configuration than a gimbaled sensor configuration. In order to accommodate the missile body motion, a wider field of view and accorate LOS must be provided for closing guidance.

Proportional guidance is quite effective and is employed in most homing weapons. By nulling the rate of the LOS to a constant velocity target, the missile travels to the intercept point in a straight line. The miss distance from an accelerating target can approach zero. A gimbaled seeker for proportional guidance need not measure angle and can have sizeable bias and scale factor errors for rate measurement. Proportional guidance places the highest demands on a body fixed sensor. A body fixed sensor must provide successive angle measurements from which the LOS rate relative to the body is computed. The body rate, which has several times the magnitude of the LOS rate, must be measured gyroscopically (star tracker is impractical) and added to obtain the LOS rate. This mechanization requires the seeker to make angle measurements with high accuracy and low noise at a high sample rate.

In summary, we have described three homing methods and the inclusion of body fixed and gimbaled sensors. Pursuit guidance is the simplest to implement with a body fixed sensor but it has difficulty with accelerating targets and crossing targets. Closing guidance is more effective than pursuit guidance but it places more demands on the body fixed sensor for a wider field of view and more accurate angle measurements. Closing guidance appears to be a logical first choice for application of the second generation FLIR's to homing applications. For conventional FLIRS, proportional guidance, with gimbaled sensors, is still the favored appraoch. A major problem in using proportional guidance with a body fixed sensor is that of obtaining target position relative to the missile velocity vector, so that lead angles can be developed.

3.0 INTELLIGENT HOMING

There are a number of issues and related work which must be addressed in the development of intelligent homing beofre we proceed with the processing of images from the NV&EOL data set. Section 2.0 was developed to provide a systems scenario for these issues.

3.1 RELATED WORK

Referring to Figure 2-2, we note that to achieve a maneuver footprint of 600 meters and given a maximum turning rate for our assumed weapon, the maximum detection and classification ranges are 2.7 km and 1.6 km respectively. The required search field is 14^{o}. If the weapon steers straight in to 1.6 km, i.e. does not initiate steering on some target, the ground coverage will be reduced 40 percent to 360 meters. If one second is allowed for classification, then steering on the target will commence at 1.1 km and the effective ground range is reduced again to approximately 248 meters. Hence, following this scenario, the ground coverage has been reduced by 41 percent and more weapons are required to increase the ground coverage toward the required amount. Unfortunately, the increase in number of weapons is non-linear because of the statistics of ballistics dispersion. There are several complementary approaches followed by the services to overcome this problem.

One approach is the development and fabrication of a high density focal plane array FLIR: one estimate indicates that 2-3 km is an achievable recognition range. With this device, recognition could occur at 2.7 km or longer (Figure 2-2) and thus allow the required 600 meters of ground coverage.

A second approach is the Advanced Pattern Matching Program of NV&EOL which requires the incoming weapon to pattern match on the background of "fresh" reconnaissance data, and steer the weapon into a "basket". In terms of Figure 2-2, we define the basket to be 1.6 km from the target and centered on the

target. Thus as the weapon closes to 1.1 km, and as it performs classification, the target is still within the coverage. Hence, for this example, the pattern matching algorithms would reduce the ballistic uncertainty from 600 to 248 meters.

Both of these approaches, defined in terms of Figure 2-2, would allow the weapon to begin classification at or longer than 1.6 km from the target. We now describe an approach which would allow the weapon to begin steering on the target during the detection phase. This approach is complementary to the above two programs.

3.2 EXTENDING GROUND COVERAGE

As can be seen from Figure 2-2, the ground coverage is maximized if target steering can be initiated during the detection phase, i.e., from 2.7 to 1.6 km. These numbers represent our model weapon. With a Focal Plane Array FLIR and use of the Advanced Pattern Matching techniques these numbers would be extended, with a consequent increase. However, there would still be a detection phase, and further increased ground coverage could be achieved if target steering were initiated during the detection phase.

At 2.7 km from the target, (Figure 2-2) detections are generated. Under the condition of a massive armor attack, described in Section 2.0, a number of detections will be found in the field of view. Some of these detections will be target detections, others will be false alarms. Of the latter, there are two general types: (1) those that persist, and (2) those that do not. Under a persistence criterion, alluded to in the Second Quarterly (Section 1.1), the latter category of false alarms can be virtually eliminated, in our experience. This is because, in closing from detection to classification range, there are 13 frames, 6 cued frames per second, of detections to correlate cued-frame to cued-frame.

In addition, there is the possibility of target prioritization based on motion. Since we assumed a massive armor attack, it is likely that the targets are moving. Furthermore, the attacking vehicles are probably not going to stop even when they come under a counter-attack. The 13 frames, collected over the 2.2 seconds from detection to classification, can be registered, processed for change detection, and for kurtosis. This might allow the weapon to discriminate between moving vehicles and those which have already been hit and are stationary. At maximum cross track velocity, a tank could travel 120 pixels during the 2.2 seconds, hence change detection is viable. False alarms then would comprise those detections which do not persist, or if they do persist, do not have significant motion with respect to other detections within the field of view.

The possibility of beginning target steering at the detection range rests on techniques such as change detection, cueing, and kurtosis - histogram analysis which we have already developed in the intelligent tracking phase of this work. We now consider another important aspect of intelligent homing, namely aimpoint selection.

3.3 AIMPOINT SELECTION

Aimpoint selection has to do with selecting a point on the target at which to aim. This is important for several reasons. There may be a particularly vulnerable portion of the target, the weapon may have a limited capability warhead which requires more accurate aiming, and the weapon steering may require the selection of a particular limited area of the target to prevent the steering system from oscillating about the target. The aimpoint discussion is broken down into two parts: (1) aimpoint selection based on exterior features, and (2) aimpoint selection based on interior features.

3.3.1 Exterior Based Aimpoint Selection

The exterior based aimpoint selection process is based on simple moment measurements of the binary pattern that is produced by the frame-to-frame tracker. Use of a binary representation is one of the reasons we went to some lengths to demonstrate the tracking capability of the cuer-binary tracker combination. Pixels representing the target are replaced with an array of logical "1"'s; all other pixels are zeroed. Necessary inputs to the aimpoint selector are target class and aspect. At this point we refer to the discussion of Section 2.0 and place these two requirements within that context.

Aimpoint selection depends on classification which may be achieved at 1.6 km from the target, according to Section 2.0. Classification could occur at longer ranges based on a higher resolution sensor and/or a higher signal to noise ratio. Further, for moving targets the location of the engine hot spot and the direction of target motion can aid classification at longer ranges. It may be possible to quantify the reliability of a classification at longer range based on the particular features employed and the persistence of a particular classification. In the case of low probability classification; steering on the group envelope seems an appropriate strategy. Since the intelligent homing system includes a cuer, classification will occur as soon as the cuer makes a classification. Aspect determination is not necessarily an output of classification.

Consider a simple case where the cuer has classified a target and is heading directly for the target. That is, the azimuth angle between the weapon and target is zero. The problem is to determine the target aspect. Consider a tank moving left to right across the field of view. The hot engine produces a bright spot on the target, so the rear of the target is identified. If the slopes of the target edges, measured in the image plane, are 90^{o} and 0^{o}, the target is aligned with the sides of the image. If the slopes are 120^{o} and 30^{o},

then the target is rotated 30^{o} in the image plane. Thus the slopes of the target edges give an approximate idea of the rotation of the target in the image plane. Length to height ratios also impart information with regard to the target rotation in a plane containing the line of sight; and parallel to the target ground plane; this plane is perpendicular to the plane of the image. This approach has some value in weapons such as Copperhead and Hellfire which are roll stabilized and either the roll or roll rate is known to a few degrees. For the missiles which are not roll-stabilized e.g. the longer range strategic weapons, the trajectory and their terminal "baskets" are such that they are coming in almost vertically and a top view of the target is presented. It should be mentioned that these vertical ballistic trajectories present problems under conditions of low cloud cover. We will present examples of aspect determination in Section 4.0.

Prior to the mission, the aimpoint is determined by analyzing the target's vulnerable area for the most likely mission scenario. Once determined, the aimpoint information is stored in terms of a feature vector, F, for each class of target , and for several aspects. During the mission, a target is detected, classified, and its aspect determined. The aspect data are used to select a feature vector from memory for that class of target and an aimpoint is computed on the actual target to be hit.

The feature vector is constructed by forming a silhouette of the target for a typical aspect angle. Here the silhouettes can be divided between those typically seen by a low-flying, roll stabilized weapon and those top views seen by a ballistic weapon with a near vertical descent.

Referring to the former, Figure 3-1 shows principal pattern axis drawn on a tank and a desired aimpoint selected. The offsets of the aimpoint from the four intersections of the target with the principal axes (R1-R4) as well as the perpendicular offsets from the pattern centroid (R0) define the aimpoint. These offsets, along with the major axes of the pattern, define the feature vector.

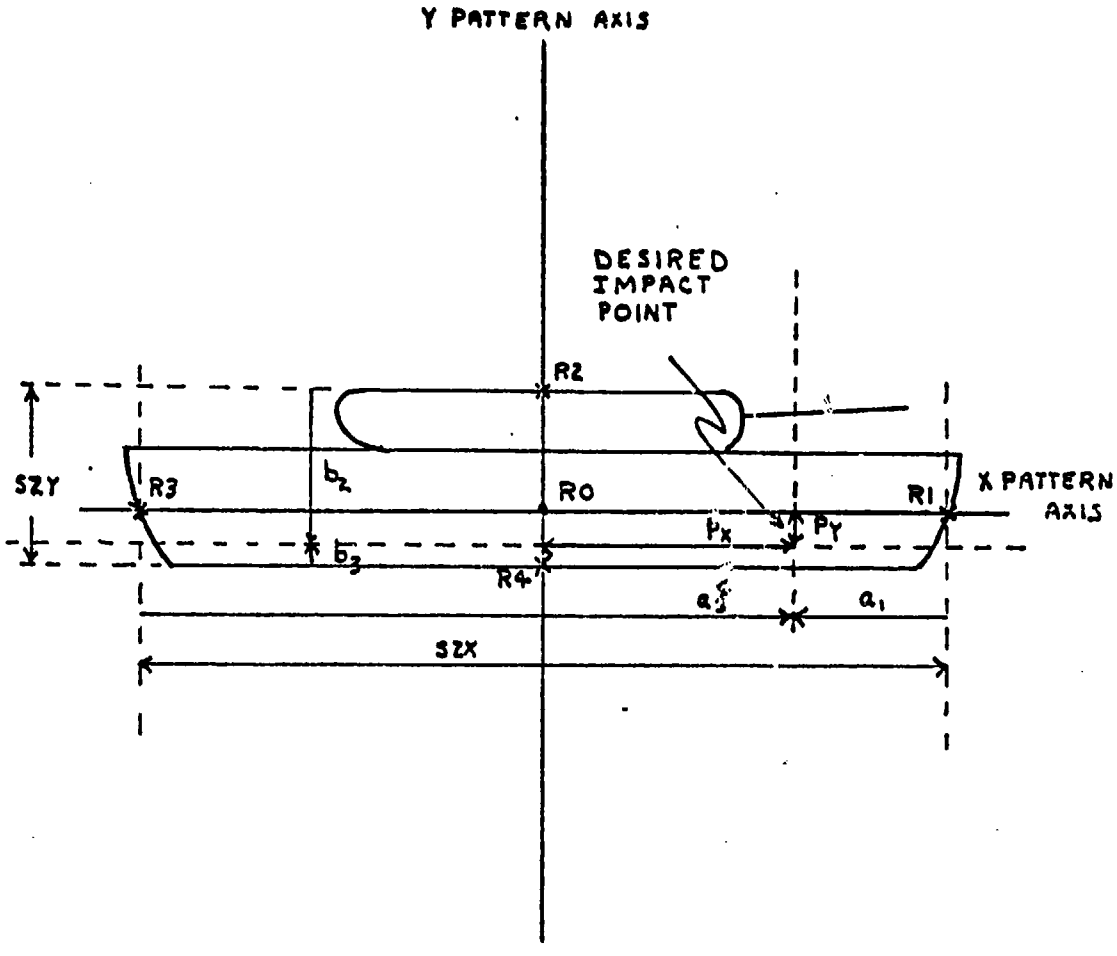

$$\overline{F} = (SZX, SZY, a_1, b_2, a_3, b_4, P_x, P_y)$$

Figure 3-1. Aimpoint Specification

The binary target pattern, used by the tracker, forms the basic input to the aimpoint processor. The first step is to perform some simple measurements on the pattern. These are the first central moments, second central moments, and joint moment :

$$\bar{X} = \frac{1}{U} \sum_{j=1}^{n} \sum_{i=1}^{n} j \; P_{ij}$$

$$\bar{Y} = \frac{1}{U} \sum_{j=1}^{n} \sum_{i=1}^{n} i \; P_{ij}$$

$$\sigma_x^2 = \frac{1}{U} \sum_{i=1}^{n} \sum_{j=1}^{n} j^2 \; P_{ij} - \bar{X}^2$$

$$\sigma_y^2 = \frac{1}{U} \sum_{i=1}^{n} \sum_{j=1}^{n} i^2 \; P_{ij} - \bar{Y}^2$$

$$\sigma_{xy} = \frac{1}{U} \sum_{i=1}^{n} \sum_{j=1}^{n} ij \; P_{ij} - \bar{X} \bar{Y}$$

$$U = \sum_{i=1}^{n} \sum_{j=1}^{n} P_{ij}$$

where n is the pixel dimension of the active area and $P_{ij} = 1$ for target pixels and $P_{ij} = 0$ for non-target pixels within the active area. The expressions for $\bar{X}$ and $\bar{Y}$ define the coordinates of the pattern centroid (X,Y). This will be the origin of the principal pattern coordinate axes. The quantities σ_x^2 and σ_y^2 define the pattern variances along the x and y axes in sensor coordinates. The quantity σ_{xy}^2 is the pattern covariance. Using the variance and covariance measurements, the angle that the principal axes of the pattern subtend with the

axes of the sensor (Figure 3-2) is given by

$$\Theta = \tfrac{1}{2} \tan^{-1} \left[\frac{2\sigma_{xy}}{\sigma_y^2 - \sigma_x^2} \right].$$

with this information, it is possible to compute the variances along the pattern axes (x', y' coordinate system).

$$\sigma_{x'}^2 = \sigma_x^2 \cos^2 \Theta - \sigma_{xy} \sin 2\Theta + \sigma_y^2 \sin^2 \Theta$$

$$\sigma_{y'}^2 = \sigma_x^2 \sin^2 \Theta + \sigma_{xy} \sin 2\Theta + \sigma_x^2 \cos^2 \Theta$$

The computations for $\sigma_{x'}^2$, $\sigma_{y'}^2$ are based on the rotational transformation of the i,j coordinates (x,y system) into i',j' coordinates (x',y' system) using standard techniques. Also used is the fact that $\sigma_{x'y'} = 0$, by definition, in the x',y' system.

To find the target size, we must find those pixels contained in and at the edge of the binary image which lie along the principal axes. These are shown as pixels R_1', R_2', R_3', and R_4' in Figure 3-2. These four intersection pixels along with the centroid, in principle axes coordinates, correspond to the set of five reference points, in image plane coordinates, described earlier.

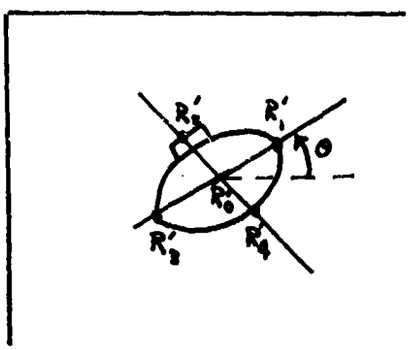

Figure 3-2. Orientation of Axes and Target

Size ratios are computed as the ratio of the measured size (SZX', SZY') for the current pattern to the stored sizes in the feature vector F:

RSX= SZX'/F(1)

RSY= SZY'/F(2),

where SZX' = $|R_1' - R_3'|$ and SZY' = $|R_2' - R_4'|$ in the current pattern and F(1) = $|R_1 - R_3|$, F(2) = $|R_2 - R_4|$ represent the reference pattern.

The next step is to generate estimates of the aimpoint location; an ensemble of five aimpoint estimates are computed. These are based on pairs of reference points R_0, R_1, $\cdots$ R_4 with one of the pair constrained to lie on the x' axis and the other on the y' axis. Figure 3-3 shows the pairs where F(1), F(2), $\cdots$ F(8) refer to SZX, SZY, a_1, b_2, a_3, b_4, P_x, P_y respectively from Figure 3-1. Note that F(1) = SZX, $\cdots\cdots$ F(8) = P_y. From this ensemble of five aimpoint estimates,$\{(AP_{xi}, AP_{yi})\ i = 1,5\}$ a composite aimpoint can be determined.

REFERENCE	x' COORDINATE	y' COORDINATE
R0, R1	RSX F(7)	RSY F(8)
R1, R2	R1 + RSX F(3)	R2 + RSY F(4)
R1,R4	R1 + RSX F(3)	R4 + RSY F(6)
R3, R2	R(3) + RSX F(5)	R2 + RSY F(4)
R3, R4	R3 + RSX F(5)	R4 + RSY F(6)

Figure 3-3. Tabulation of Reference Point Pairs and Corresponding Aimpoint Estimates in Terms of Size Ratios, Reference Point Locations and Stored Data

A few comments concerning redundancy are in order here. If the pattern formation and measurement processes are perfect and noise free, then all five aimpoint estimates should be degenerate. These preconditions however, are most unlikely to occur. Therefore, it is expected that, at the very least,

two or more estimates will be different. The aimpoint ensemble may be thought of as defining an area on the target pattern. A composite aimpoint can be computed as the arithmetic or weighted mean over the ensemble. Before this is done, a simple test for ensemble members is to determine if they lie within the binary pattern. It should be noted that the RSX and RSY allow the aimpoint estimate to be updated with decreasing range.

As the range closes, the target becomes larger and larger and the tracker must handle a larger and larger track window. Preliminary estimates seem to indicate that a 64x64 pixel window will require special computation procedures which take more time and yield results which are not as reliable as those achieved with the more straight-forward computations for smaller windows. Hence, based on limitations of the frame-to-frame tracker, a 64 pixel target appears as a natural transition to aimpoint selection based on interior features.

3.3.2 Interior Based Aimpoint Selection

Based on the analysis of Section 2.0, and the above constraint, the range has closed to approximately 200 meters (for target side view) when the aimpoint selection technique switches from exterior to interior features. At 500 meters/second, the time to impact is 0.4 sec and 12 frames of data are available. At 27 meters from the target, the target image fills the field of view.

An issue here is that range at which the intelligent homing system is constrained to concentrate on only one target. Again from Section 2.0, we note that the guidance settling occurs in the last 500 meters to the target. In the region from 1.6 km to 0.5 km, the intelligent homing system can track all the targets within the field of view and must commit itself to the highest priority one before the 500 meter mark is passed. Consider now some characteristics of the aimpoint based on interior features.

Clearly, the aimpoint should represent some vulnerable area. From the standpoint of image processing, the aimpoint should be a high contrast region with regard to the rest of the target. It should be repeatable from frame-to-frame and not scintillate or fluctuate.

In conclusion, we feel that the interior aimpoint selection problem is not one of identifying the desired point out of context. Rather, the target has been classifed, the aspect has been determined, and an aimpoint based on exterior features selected. The aimpoint selection based on interior features should be in approximately the same location as the former and more time will be allotted for the calculation. That is, from 500 meters until 27 meters to impact, the entire field of view need not be processed.

4.0 PRELIMINARY RESULTS

This section is divided into two parts: (1) long range aimpoint selection and homing, and (2) close-in aimpoint selection and homing. Further, the transition region between the two and the reasons for the dichotomy are discussed. Three examples from the NV&EOL data base are presented.

4.1 LONG RANGE AIMPOINT SELECTION

Long range aimpoint selection is based on the technique described in Section 3.3.1, Exterior Aimpoint Selection. At long range, the exterior shape is a reliable and repeatable feature. This section provides an example of long range aimpoint selection taken from the NV&EOL data base described in the First Quarterly Report. Section 2.2.5, Tape #5, 11/15/77, Tape Position 5280 is a side view of a tank moving perpendicularly to the field of view from right to left.

The median filter was deleted in this example only because we were looking for a small engine hot spot in the segmentation process. Hence, the aimpoint selection and tracking are based on the binary values resulting from the segmentation processes described in previous quarterlies with the deletion of the 3x3 median filter for this example only. The model for the aimpoint selection is shown in Figure 4.1-1a.

In Figure 4.1-1b, we have arbitrarily assigned values to each of the eight members of the feature vector. We place the coordinate system at R_0 and the directions along the principal axis are the same as the sensor coordinate system: i.e., down is positive and left to right is positive as shown in Figure 4.1-1a. In this coordinate system, R_3 and R_2 have negative coordinates $(-x',0)$ and $(0,-y')$ respectively, while R_1 and R_4 have positive coordinates. Figure 4.1-1b shows the quantities for the reference vector; note that some of the quantities are signed values indicating direction. The aimpoint is labelled AP and shown with an asterisk (*).

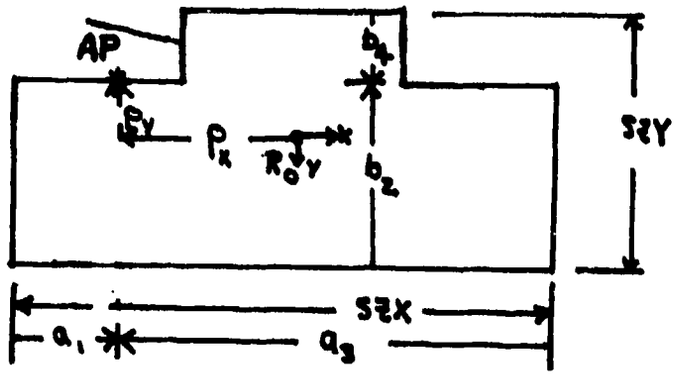

Figure 4.1-1a. Principal Axes Directions.

FEATURE VECTOR

F(1)	=	SZX	=	4
F(2)	=	SZY	=	3
F(3)	=	a_1	=	+1
F(4)	=	b_2	=	+2
F(5)	=	a_3	=	-3
F(6)	=	b_4	=	-1
F(7)	=	P_x	=	-1
F(8)	=	P_y	=	-.5

Figure 4.1-1b. Reference Quantities

The following figures show the binary target shape from the frame-to-frame tracker, described in Section 1.0 and previous Quarterlies, for consecutive images 224, 228, 232, 236, 240, 244, 248, 252, 256, and 260. The aimpoint calculations are shown below each shape and the aimpoint is superimposed on the target silhouette. We describe the aimpoint computation for image 224 in some detail

and then present the remainder of the images and their aimpoint computations. Image 224 is shown in Figure 4.1-2. The first and second central moments are:

$$\bar{X} = XBAR = \frac{1}{U} \sum_{j+1}^{n} \sum_{i=1}^{n} j\, P_{ij}$$

$$\bar{Y} = YBAR = \frac{1}{U} \sum_{j=1}^{n} \sum_{i=1}^{n} i\, P_{ij},$$

where $U = \sum_{i=1}^{n} \sum_{j=1}^{n} p_{ij}$, and i and j are the row and column numbers starting from the upper left-hand corner of the track window. The first central moment is computer on a binary image by summing the number of "1" pixels in each column and multiplying by the column number. These products are then summed and divided by the number of "1" pixels in the image. Thus,

$\bar{X} = XBAR = \frac{1}{156}[10x6 + 11x6 + 12x9 + 13x9 + ...] = 17.78$ and,

$\bar{Y} = YBAR = \frac{1}{156}[6x6 + 7x4 + 8x12 + 9x14 + ...] = 1888/156 = 12.10$. The variances,

$$\sigma_x^2 = \frac{1}{U} \sum_{i=1}^{n} \sum_{j=1}^{n} j^2\, P_{ij} - (XBAR)^2$$

$$\sigma_y^2 = \frac{1}{U} \sum_{i=1}^{n} \sum_{j=1}^{n} i^2\, P_{ij} - (YBAR)^2$$

can be evaluated in a similar fashion as well as the expression for the joint moment, σ_{xy}. The XBAR, YBAR pixel truncated to (17, 12) is shown circled in Figure 4.1-2. We note that σ_x, σ_y provide a rough measure of the target extent in the x,y directions as measured by the coordinates of the image plane. The angle that the principle axis makes with the image coordinate system is found

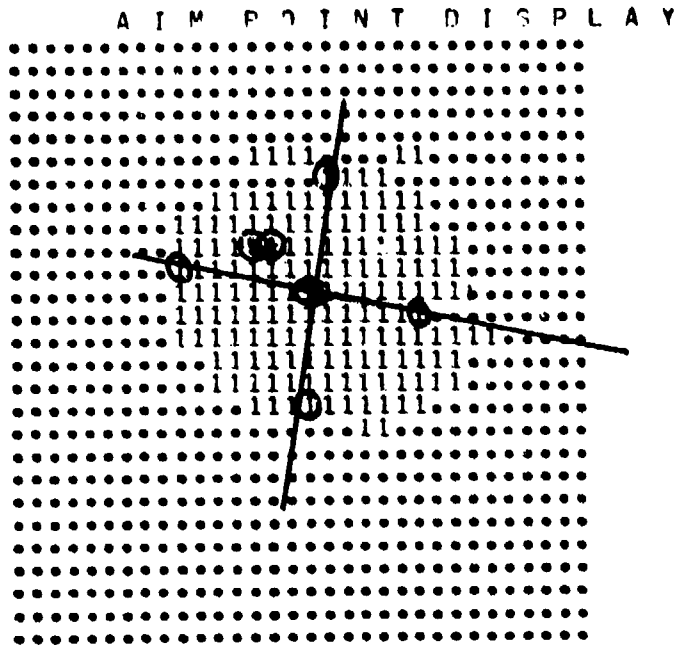

XBAR = 17.782
YBAR = 12.103
SIG2X = 18.094
SIG2Y = 9.425
SIGXY = 1.227
THETA = -7.907
SIG2XP = 18.264
SIG2YP = 9.255
R0 = 17 12
R1 = 23 13
R2 = 18 7
R3 = 10 11
R4 = 17 17

AIM POINTS

-3.250 1.667

-3.750 1.667
-3.750 1.667
-3.750 1.667
-3.750 1.667

Figure 4.1-2. Image 224 and Aimpoint Computations

by substituting into

$$\Theta = \tan^{-1}\left[\frac{\sigma_{xy}}{\sigma_y^2 - \sigma_x^2}\right] = \tan^{-1}\left[\frac{1.227}{(9.425-18.094)}\right]$$

and

$$\Theta = -7.9^{0}.$$

Thus by a rotation,

$$x' = x\cos\Theta - y\sin\Theta$$

$$y' = -x\sin\Theta + y\cos\Theta,$$

a point along the image plane axes can be mapped into a point along the principal axes. The coordinates of the perimeter points along the principal axes can be found from this equation. In fact, all four perimeter points are shown in Figure 4.1-2 as circled pixels along the principal axis. In order not to clutter Figures 4.1-2, the perimeter points R_1', R_2', R_3', and R_4' are shown in Figure 4.1-3 with R_0', the centroid. These pixels correspond to those of the model target shown in Figure 4.1-1a.

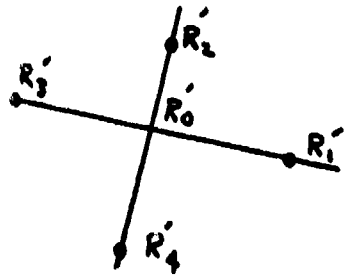

Figure 4.1-3. Location of Principal Axis - Perimeter Pixels

The next step is to determine the size of the actual target with respect to that of the model. In hydrodynamic modelling, this is the constant of proportionality. From the actual target, image 224, SZX' = $|\acute{R1} - \acute{R3}|$ and SZY' = $|\acute{R2} - \acute{R4}|$

$$SZX' = [\,(23-10)^2 + (13-11)^2\,]^{1/2} = 13.2$$
$$SZY' = [\,(18-17)^2 + (17-7)^2\,]^{1/2} = 10.1,$$

and the model target has SZX = 4, SZY = 3. Hence the constants of proportionality are RSX = SZX'/F(1), RSY = SZY'/F(2) which becomes 3.25 and 3.3, respectively.

Now, we compute five estimates for the aimpoint based on various combinations of R_0, R_1, R_2, R_3, and R_4. The five sets of coordinate expressions are described in Section 3.3.2 and the appropriate numbers for this example are shown in Figure 4.1-4. Note that the aimpoint coordinates are referenced to the target centroid, but they are measured along the x,y axis centered at the centroid instead of the x', y' axis for the illustrations.

REFERENCE	X' COORD	Y' COORD
R_0, R_1	RSX • F(7) = 3.25 x -1	RSY • F(8) = 3.3 x 0.5
R_1, R_2	R1 + RSX • F(5) = 6 + 3.25 x (-3)	R_2 + RSY • F(6) = +5 +3.3 x (-1)
R_1 , R_4	R_1 + RSX • F(5) = 6 + 3.25 x (-3)	R_4 + RSY • F(4) = .5 + (3.3) x (+2)
R_3, R_2	R_3 + RSX • F(7) = -7 + 3.25 x (+1)	R_2 + RSY • F(6) = +5 +3.3 x (-1
R_3, R_4	R_3 + RSX • F(7) = -7 + 3.25 x (+1)	R_4 + RSY • F(4) = .5 + (3.3) x (+2)

Figure 4.1-4. Aimpoint Coordinates in X', Y' Coord.

Having described the first example in some detail, we now proceed with the following images in the series noting that they are tracked by the frame-to-frame tracker and the aimpoint is computed from the tracker binary reference image.

Figures 4.1-5 through 4.1-13 show the aimpoint computations for images 228, 232, ... 260. In general, four of the aimpoints cluster very well, while the one based on the target centroid is consistently off by one to three pixels. Further, the aimpoint computations are putting the aimpoint in the upper left-hand portion of the target as the template requires in Figure 4.1-1. There is a variance in the principal axes angle of -6 degrees to about -15 degrees. For the next Quarterly, we shall repeat several of these images using median filtered data to test for the variability of the principal axes angle with a more compact target. In conclusion, the aimpoint calculations seem to be placing the aimpoint within a few pixels of the desired point which is adequate at these ranges since there is sufficient time remaining before impact to make adjustments. It appears that majority vote is an appropriate strategy to select a single aimpoint. Note that the major reason for the congruence between the first aimpoint and the others is the compactness of the target. To the extent that outlying pixels, not connected to the main body, move the centroid from the center of the main body,

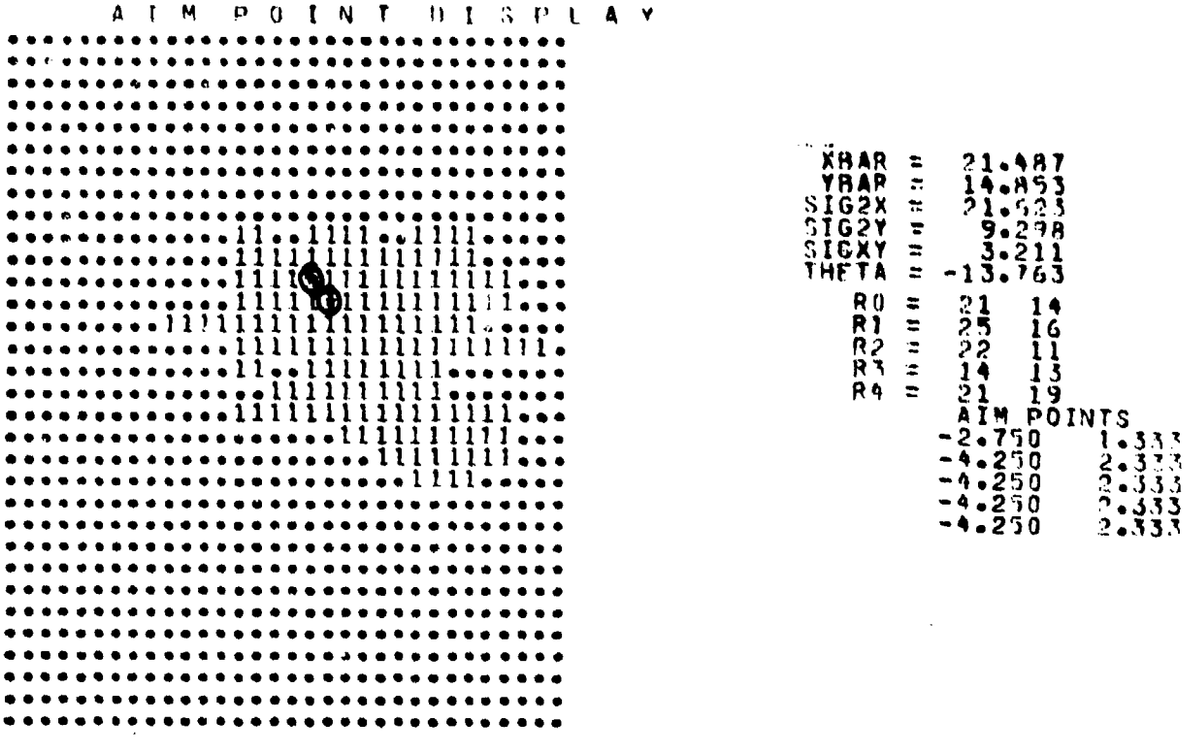

Figure 4.1-5. Aimpoint Computations, Image 228

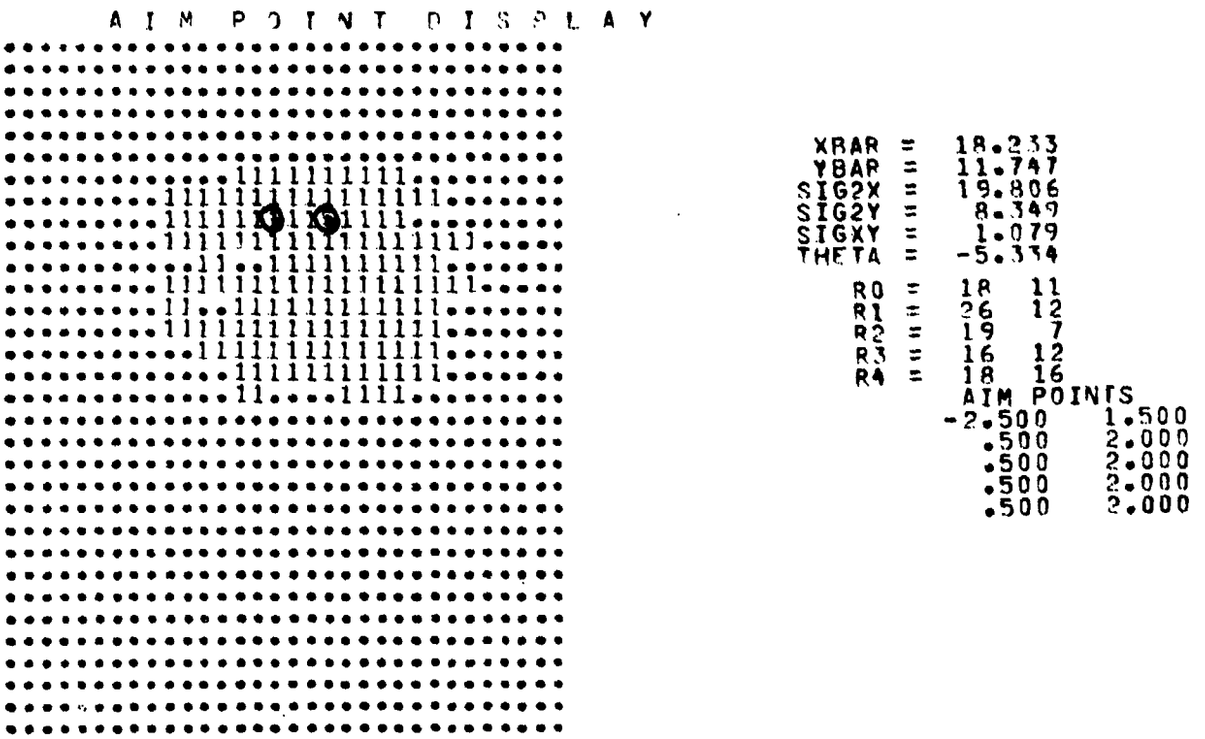

Figure 4.1-6. Aimpoint Computations, Image 232

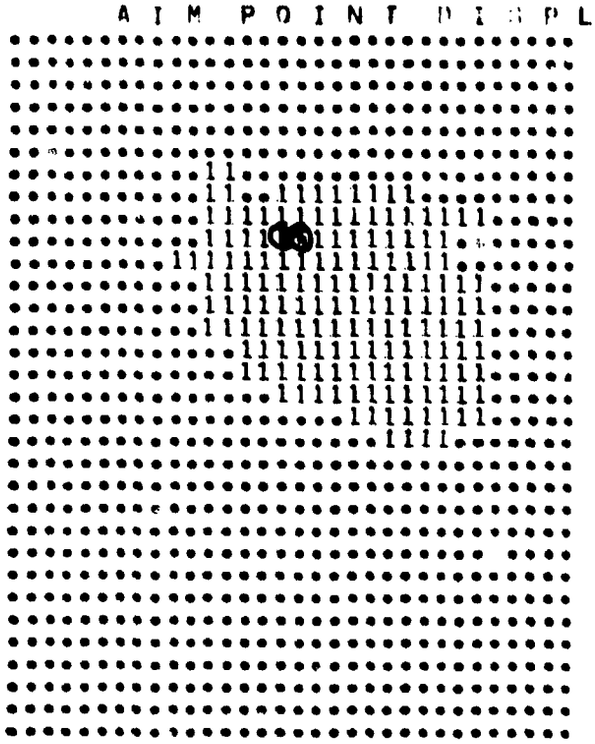

XBAR = 19.665
YBAR = 12.896
SIG2X = 19.957
SIG2Y = 9.595
SIGXY = 4.335
THETA = -19.960

R0	=	19 12
R1	=	27 16
R2	=	21 8
R3	=	12 10
R4	=	18 17

AIM POINTS

-3.750	1.500
-3.250	2.000
-3.250	2.000
-3.250	2.000
-3.250	2.000

Figure 4.1-7. Aimpoint Computations, Image 236

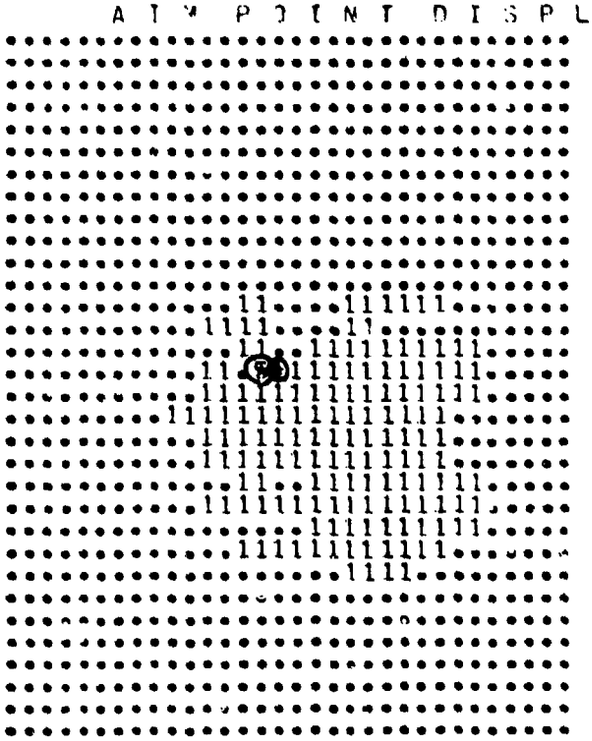

XBAR = 19.591
YBAR = 18.961
SIG2X = 18.904
SIG2Y = 10.687
SIGXY = 1.159
THETA = -7.879

R0	=	19 18
R1	=	25 20
R2	=	20 13
R3	=	10 18
R4	=	19 24

AIM POINTS

-3.750	1.833
-5.250	2.333
-5.250	2.333
-5.250	2.333
-5.250	2.333

Figure 4.1-8. Aimpoint Computations, Image 240

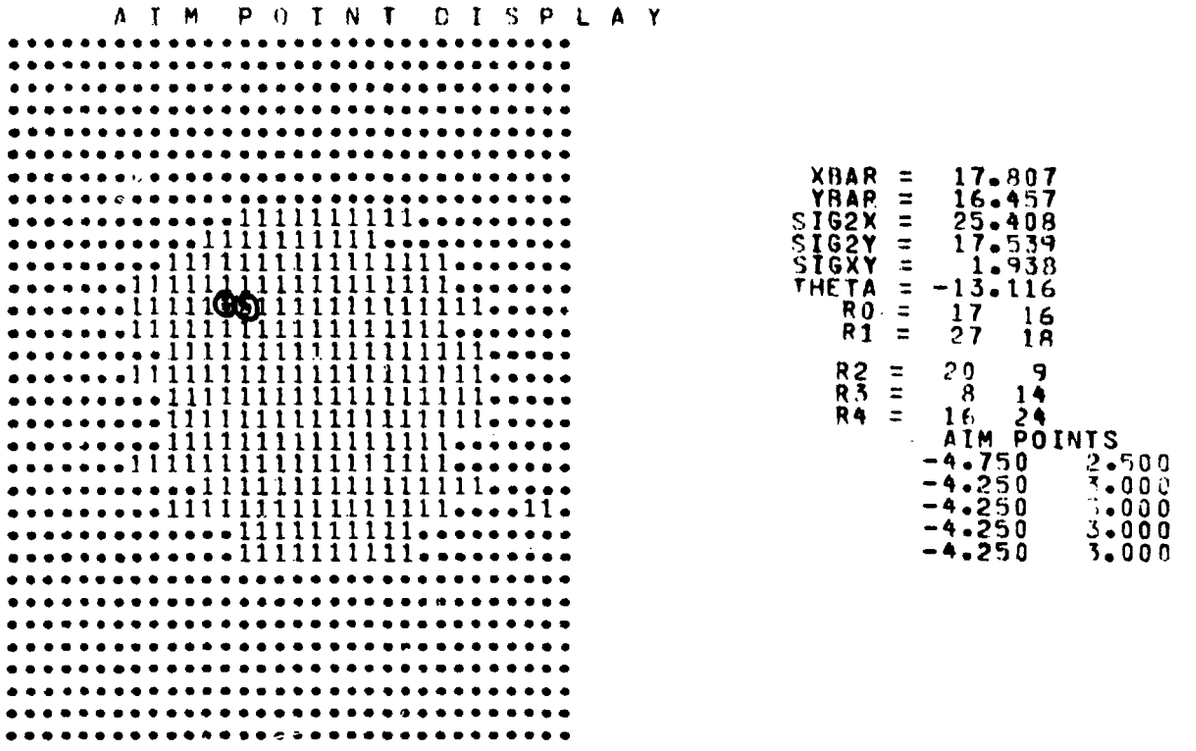

Figure 4.1-9. Aimpoint Computations, Image 244

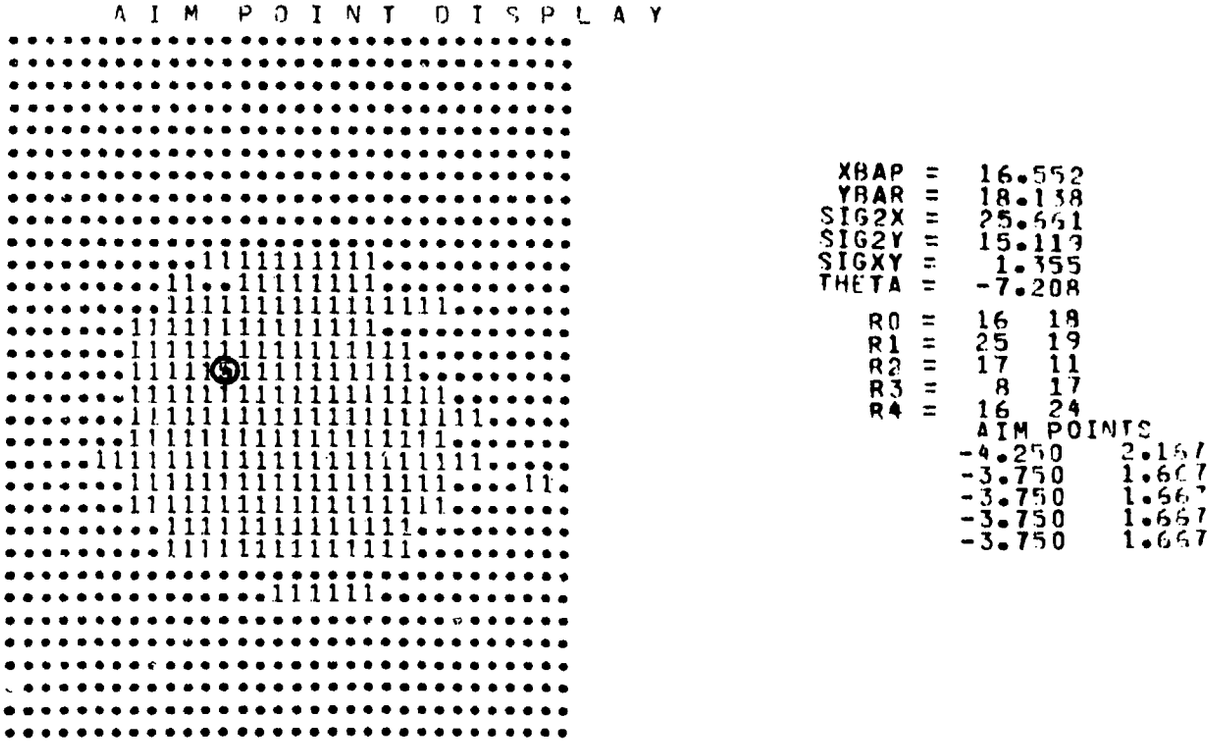

Figure 4.1-10. Aimpoint Computations, Image 248

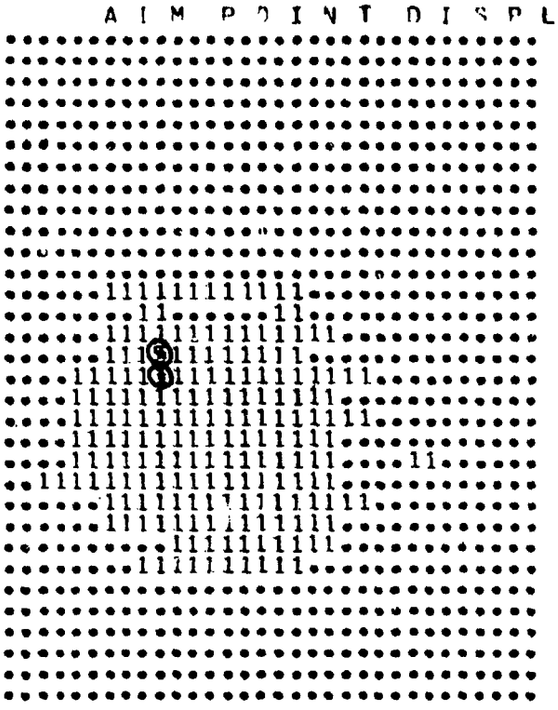

XBAR = 13.255
YBAR = 19.684
SIG2X = 21.741
SIG2Y = 13.094
SIGXY = 1.188
THETA = -7.681

R0 = 13 19
R1 = 20 21
R2 = 14 15
R3 = 5 19
R4 = 12 26

AIM POINTS

-3.750	1.833
-4.250	3.333
-4.250	3.333
-4.250	3.333
-4.250	3.333

Figure 4.1-11. Aimpoint Computations, Image 252

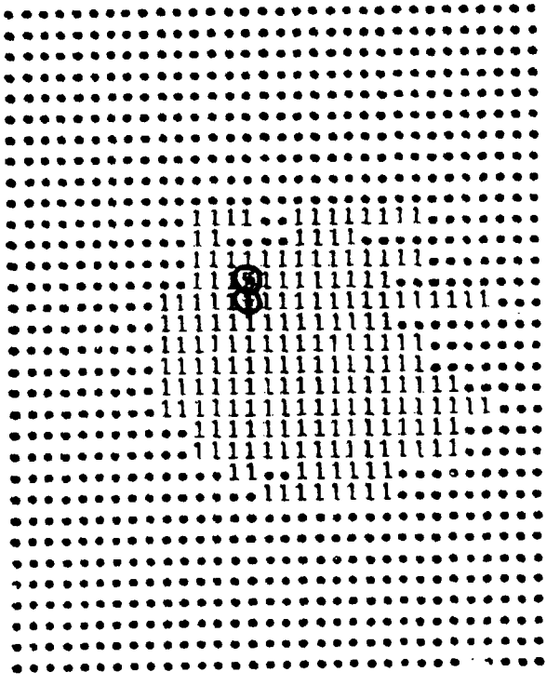

XBAR = 18.541
YBAR = 17.571
SIG2X = 22.289
SIG2Y = 13.000
SIGXY = 1.548
THETA = -9.217

R0 = 18 17
R1 = 27 19
R2 = 20 11
R3 = 10 16
R4 = 17 24

AIM POINTS

-4.250	2.167
-3.750	2.667
-3.750	2.667
-3.750	2.667
-3.750	2.667

Figure 4.1-12. Aimpoint Computations, Image 256

the aimpoint will be different. The model for the first aimpoint assumes that R_0^1 is equidistant from R_1^1 and R_3^1.

Figure 4.1-14 shows the aimpoint for images 229,228,...260 where median filtering has produced a more compact target representation.

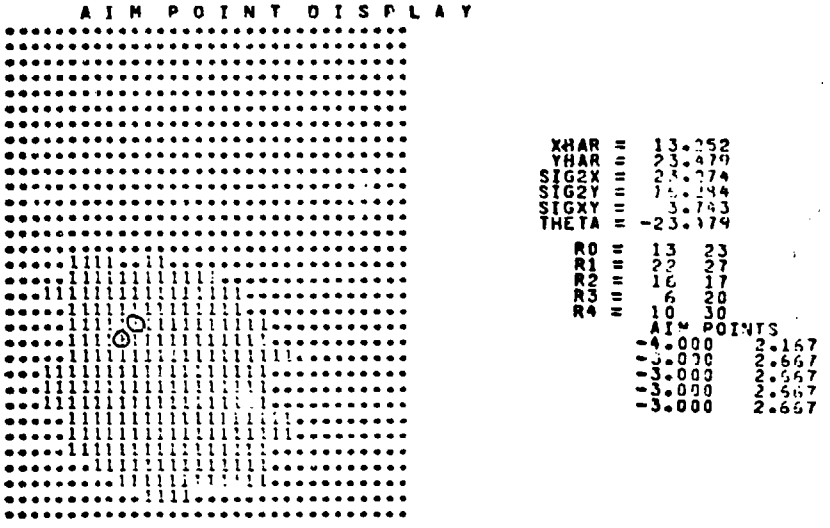

Figure 4.1 - 13 Aimpoints Computations, Image 260

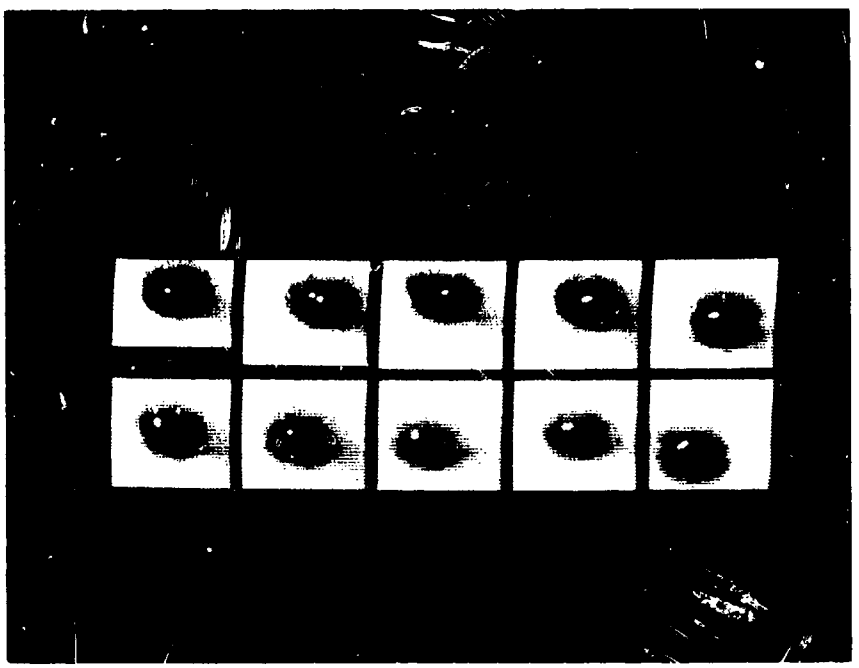

Figure 4.1 - 14. Aimpoint Computations, Images 224,...260 for Median Filtered Images

4.2 Close-In Homing and Aimpoint Selection

The purpose of this section is to discuss several preliminary problems which must be solved in order to accomplish close-in homing and aimpoint selection. The first problem is segmentation of a close-in target and the second is frame-to-frame tracking of such a target.

4.2.1 Close-In Segmentation

Segmentation of a large target, 30 lines or more, introduces several differences from segmentation of a small target. The smaller target can be segmented as a light target against a dark background or vice versa. A large target may consist of both light and dark portions; hence, segmentation techniques for large targets should be bipolar. A second difference is found in the interior, structural features which are present in the large target. These features may exhibit the "blob-like" characteristic of a small target, i.e., there exists a general decrease in gray level as one moves from the center of the blob to the edge in any direction. However, these features may also exhibit "contour-like" characteristics, i.e. the gray level does not diminish isotropically as one moves from the center but may increase in one direction and diminish in the opposite direction. As an example of close-in segmentation, we consider images from the NWC/OL 875-line data base described in the First Quarterly Report. The scenario is described in Section 2.2.5 "Tape #5 11/14/77", Tape Position 5280. The helicopter is closing on a moving tank from the rear; the tank is moving along a narrow road. We shall show in this example that it is possible to segment the target better by moving beyond the superslice threshold which gives the maximum edge/perimeter matches and consider the kurtosis (texture) ideas derived in the Third Quarterly Report. This allows us to determine target aspect which facilitates aimpoint selection. Further, by means of the same kurtosis ideas used in the disappearing and

reappearing target cases of the Third Quarterly, we can estimate the threshold at which target background merging occurs.

Figure 4.2-1 shows the segmentation for the tank at a threshold of 12; essentially, the segmented portion is the hot engine. Figure 4.2-2 shows the number of edge/perimiter matches, average gray level, average x position, average y position, width (DELX), height (DELY), total number of pixels, and number of perimeter points vs. the superslice threshold. Note from the figure that the maximum number of edge/perimeter matches occurs at a threshold of 35 and that image is shown in Figure 4.2-3. Continuing beyond the threshold for maximum edge/perimeter matches, we obtain Figure 4.2-4 at a threshold of 37. Here, we can see the beginnings of the distinctive gun barrel. Figure 4.2-5 shows the same image, thresholded at 38 and the ensuing merging with the background. Note the large jump in the number of pixels contained in the target at a threshold of 38 and the large jump in the average gray level. This jump is similar to the jump in target size for the disappearing target case when the backgournd was included in the target shape. Further, the large expansion in the target's x dimension leads one to suspect that the additions are not part of the target. An added degree of sophistication could be achieved by tracking the background blobs as they form and computing their probability of being part of the target by their additions to the target dimensions. Figure 4.2-6 is the descriptive table of target characteristics for image 1804. Almost the same thing happens again except there are several maximums in 2804. Again, they are passed on the way to the best target description.

In conclusion, it is seen that a more complete segmentation of a close-in target can be achieved by taking into account not only the maximum number of edge/perimeter matches but the average gray level across the target and the number of pixels added to the target at each gray level. In the next quarterly, we hope to reduce these heuristics to something more concrete based on further examples.

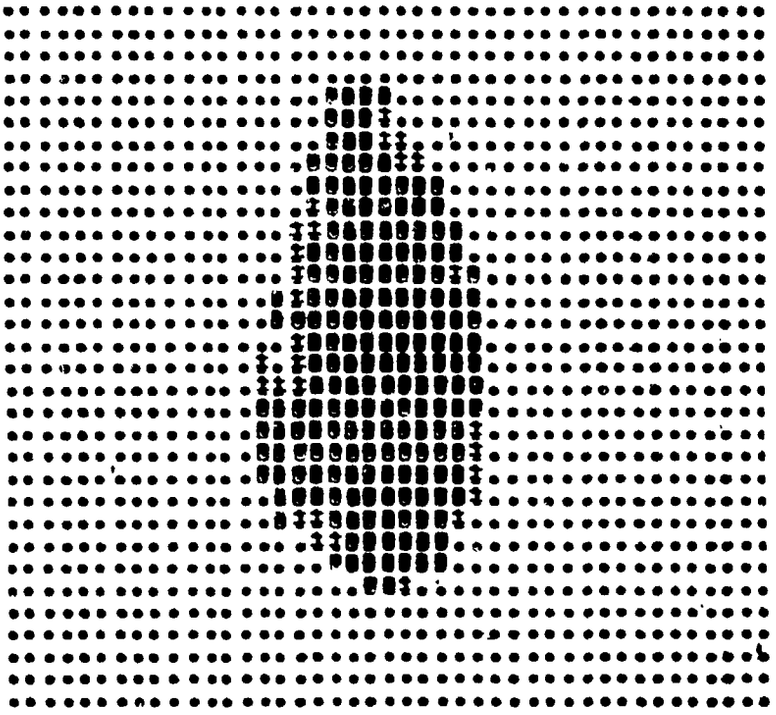

Figure 4.2-1. Segmented Target, Image 1784
Threshold = 12.

IMAGE 1784

THRESHOLD	MATCHES	AVE. GRAY LEVEL	XBAR	YBAR	ΔX	ΔY	SIZE	PERPTS
12	34	11.70	40.56	105.7	9	19	108	57
13	28	12.36	38.33	104.8	13	23	220	71
14	31	12.62	37.98	104.7	15	24	261	74
15	33	12.92	37.65	104.3	16	25	298	78
16	36	13.08	37.55	104.1	16	26	315	80
17	39	13.27	37.39	103.9	16	26	331	80
18	42	13.37	37.37	103.9	16	27	338	82
19	49	13.61	37.41	103.8	16	28	353	84
20	58	13.85	37.48	103.7	18	29	367	90
21	59	13.95	37.49	103.5	18	29	372	90
22	64	14.24	37.56	103.3	18	29	386	90
23	71	14.51	37.53	103.4	18	30	398	92
24	72	14.74	37.55	103.2	18	31	408	93
25	81	15.15	37.36	103.0	18	31	425	93
26	82	15.30	37.45	103.0	18	31	431	94
27	87	15.72	37.43	102.7	18	32	447	96
28	87	16.04	37.41	102.8	18	32	459	96
29	88	16.34	37.41	102.6	18	34	470	99
30	91	16.74	37.46	102.3	19	34	484	102
31	93	17.28	37.51	102.1	20	35	503	106
32	93	17.95	37.48	101.9	20	37	527	110
33	94	18.60	37.40	101.8	20	38	551	112
34	96	19.14	37.40	101.5	20	39	571	115
35	98	19.76	37.28	101.1	21	40	594	120
36	87	20.92	37.19	100.7	22	42	640	124
37	100	22.83	37.23	98.8	23	53	727	153
38	155 merged	27.37	32.41	102.2	39	59	1046	225
39	159	28.58	31.59	101.9	40	59	1168	227

Target 4.2-2. Target Characteristics vs. Superslice Threshold, Image 1784

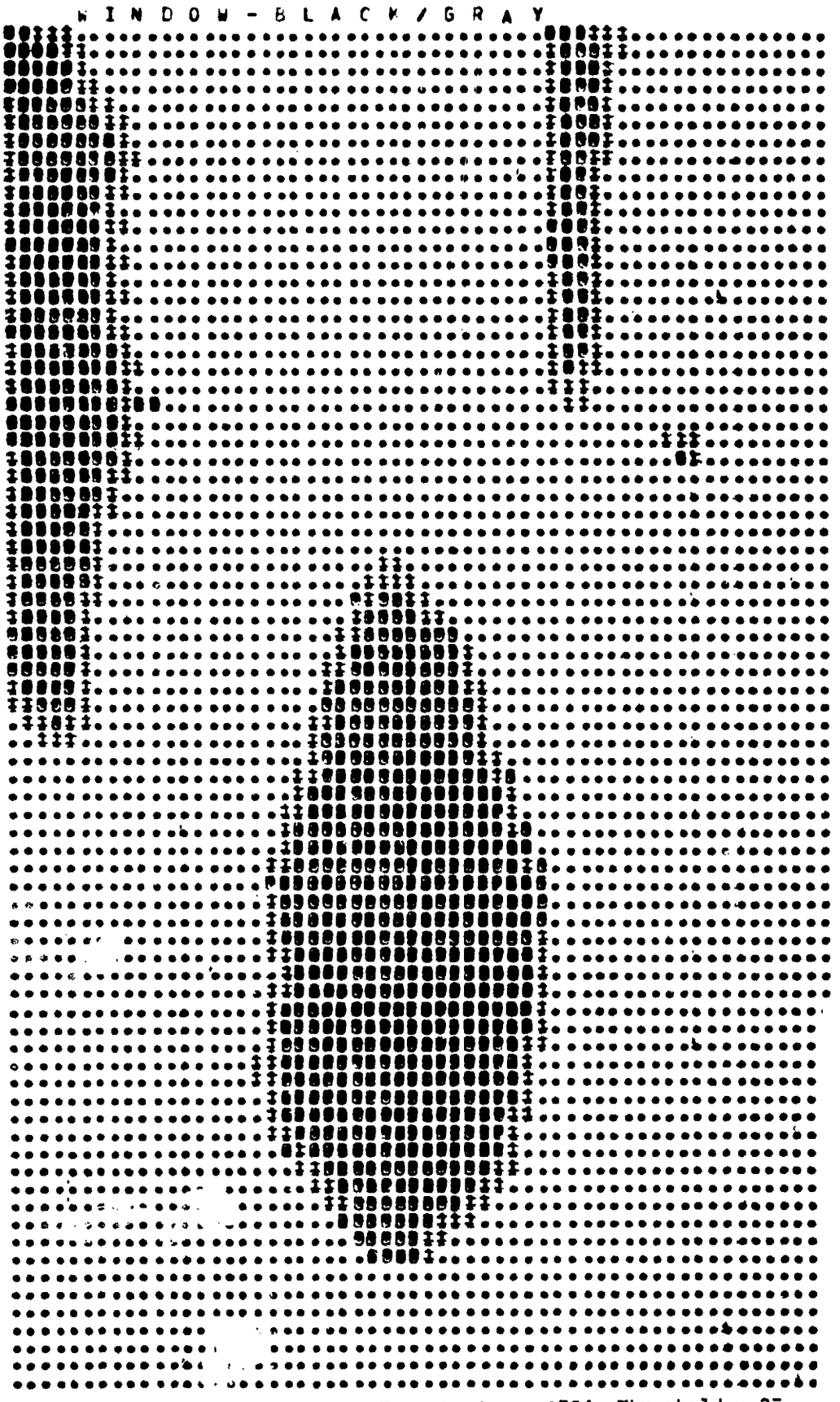

Figure 4.2-3. Segmented Target, Image 1784, Threshold = 35

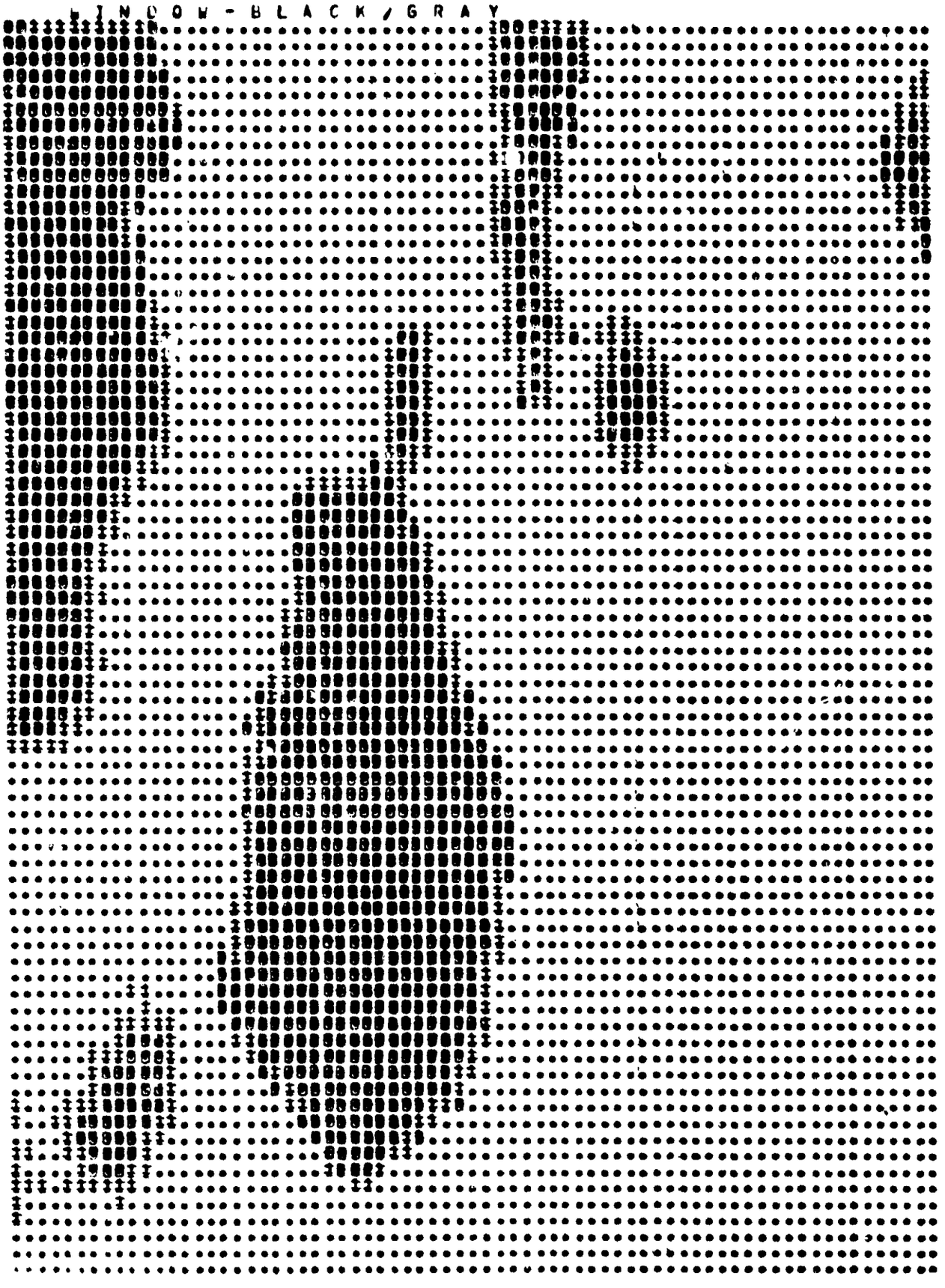

Figure 4.2-4. Segmented Target, Image 1784, Threshold = 37

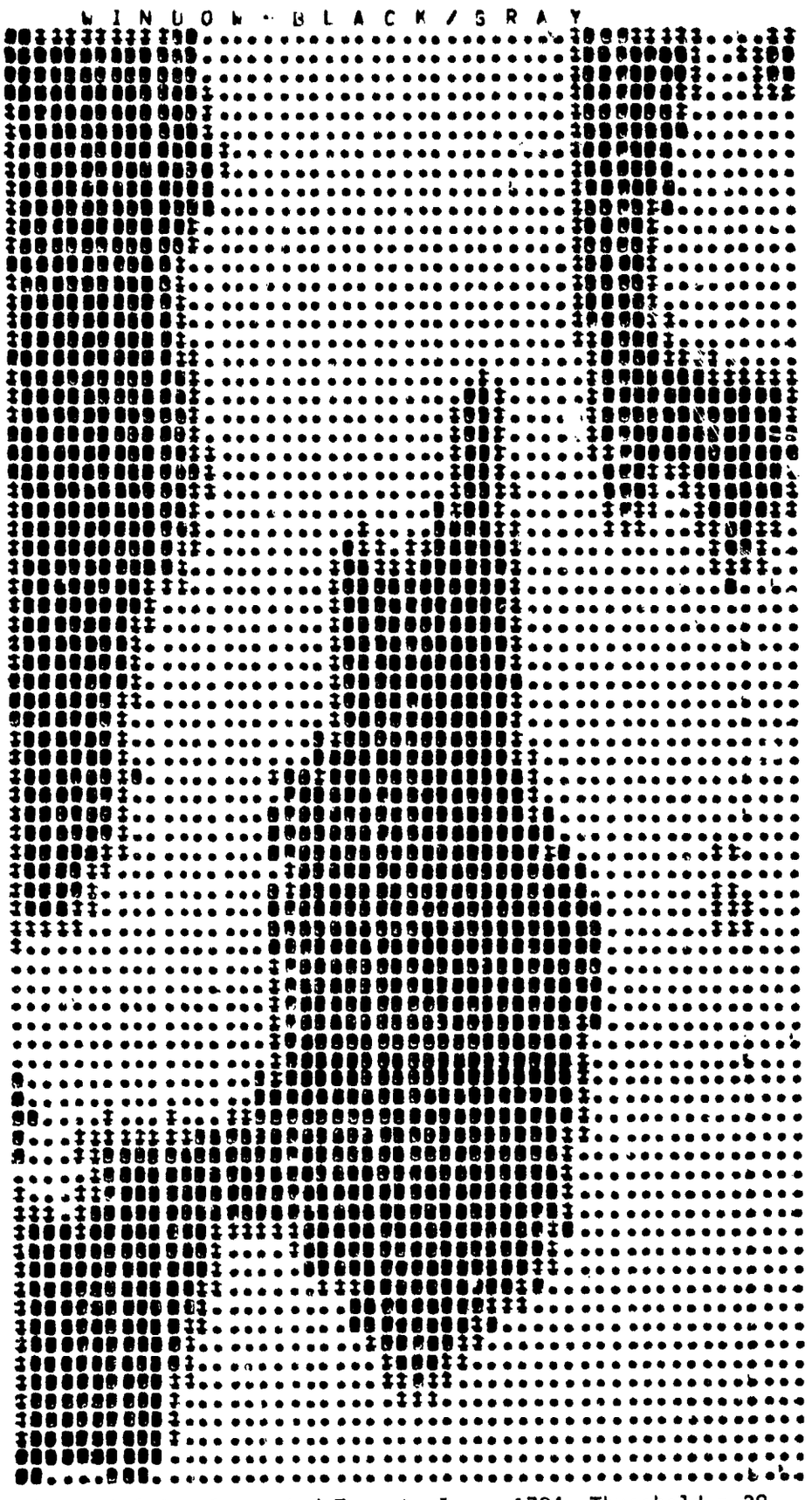

Figure 4.2-5. Segmented Target, Image 1784, Threshold = 38

IMAGE 1804

THRESHOLD	MATCHES	AVE. GRAY LEVEL	XBAR	YBAR	ΔX	ΔY	SIZE	PERPTS
12	40	11.[illegible]	40.93	99.35	11	21	164	67
13	32	12.09	39.33	98.92	15	23	261	71
14	28	12.29	38.97	98.57	16	25	292	79
15	29	12.50	38.75	98.47	16	25	316	78
16	33	12.60	38.83	98.39	17	25	326	79
17	40	12.88	38.86	98.07	17	26	398	82
18	47	13.09	38.76	98.10	18	28	363	89
19	50	13.30	38.77	97.88	18	28	376	90
20	54	13.47	38.70	97.57	18	29	386	92
21	57	13.64	38.68	97.95	18	29	395	90
22	65	13.85	38.76	97.24	18	30	405	92
23	67	14.05	38.75	97.10	18	30	414	92
24	76	14.53	38.73	97.16	19	31	435	95
25	81	14.86	38.82	96.91	19	32	449	98
26	84	15.07	38.78	96.91	19	32	458	98
27	91	15.55	38.82	96.90	19	33	477	100
28	93	15.70	38.84	96.45	19	34	483	102
29	94	16.10	38.83	96.26	19	35	498	103
30	(95)	16.48	38.78	96.10	19	36	512	105
31	93	17.03	38.79	95.96	19	37	532	108
32	91	17.57	38.90	95.52	20	38	552	112
33	90	18.34	38.88	95.30	21	40	581	117
34	(92)	18.79	38.78	95.36	21	40	598	121
35	89	19.59	38.68	94.98	21	41	629	121
36	81	20.61	38.56	99.21	21	42	671	122
37	91	22.69	38.54	92.07	25	54	769	157
38	213 merged	31.66	21.11	83.07	49	87	2568	379

Figure 4.2-6. Target Characteristics vs. Superslice Threshold, Image 1804

4.2.2 Close-In Target Tracking

Close-In Target Tracking on a frame-to-frame basis runs headlong into the existence of target contours as described in the previous section. Some of the problems in tracking an interior feature are described here. Recall, that the intelligent tracker system concept, described in Section 1.0, requires that the cuer segment the entire frame and provide a reference, gray level target image to the tracker. This reference image is binarized by the tracker under the assumption that there is a difference in gray level between the target and its immediate surroundings. The contour affects the cuer segmentation and the binarization of the tracker reference image. At the segmentation level, consider a target which has an isotropic gray level distribution for the engine hot spot and the remainder of the target consists of contours. That is, there are definable edges to the contours, but, in general the gray level darkens with distance away from the engine spot. The Superslice algorithm will segment the engine hot spot but will also include it within the target as the gray level threshold is increased and a maximum number of edge/perimeter matches is sought. Individual contours can be isolated by additional processing such as the employment of bands or ranges of thresholds. For example, recall the road crossing case in the Second Quarterly. Additionally, the number of edge/perimeter matches may achieve several local maxima before the entire target is segmented. In summary, additional processing must be added to Superslice to isolate structural features and segment the entire target. More significantly, the presence of contours affects the tracking process and the formation of a binary reference image. In Figure 4.2-7, we show such a contour with a square contained in it, shown by dashed lines. The major thrust of gray levels is from light to dark in the direction of the arrows. There is enough contrast along the vertical sides of the square to obtain the vertical, dashed edges. However, the presence of gray levels in the contour close to those gray levels within the square means that

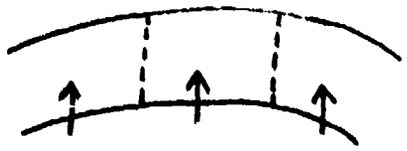

Figure 4.2-7. Track Square with Contour

the contrast across the vertical edges is low. In other words, the gray levels in the reference target background will be close to those in the reference target image (the square) and the track window may wander about the contour.

As an example, a 3x3 square just ahead of the hot engine signature was chosen by eye; this square seemed fairly repeatable in the series of images: 1784, 1788, 1792, 1796, 1800, 1804, 1808, 1812, 1816, 1820, 1824, 1828, 1832, 1836, and 1840. These are taken from the set of images described in Section 4.2.1. The square was selected on images 1784, 1804, and 1824; this selection process was a substitute for the cuer. The intervening four images 1788-1800, 1808-1820, and 1828-1840 were tracked with the binary correlation tracker described in the Third Quarterly Report. Tracking was attempted on the raw gray levels and gray levels processed with a 3x3 median filter. In both cases the results were sporadic. The problem seemed to be that the square we had chosen was really located in a contour of approximately the same gray levels as shown in Figure 4.2-7. The tracker, then could move about the contour with the accompanying change in shape of the reference as it was handed from frame-to-frame. Thus by the fourth track frame, the aimpoint shape had changed substantially. Figure 4.2-8 shows several successive track windows from the 3x3 median filtered data.

Based on this data, we decided to track over the entire segmented target as shown in the previous section using extended edges or subsets. This would allow us to take advantage of the repeatability of a large number of extended

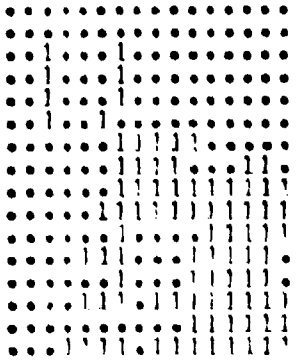

Image 1788

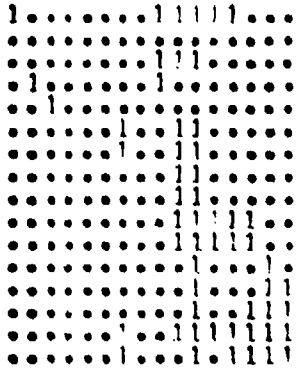

Image 1792

Figure 4.2-8. Successive Track Images,
Binary Correlation Tracker

edges contained in the target. Then, at the very worst, the aimpoint could be computed as previously described in the long range case. We note here that this approach is viable, assuming a program driven processor, because the projectile will probably have to settle on a single target by the time the image is 30 or so lines high (refer to Section 3). Hence, there is no need to scan the entire field at this point. To prove feasibility of frame-to-frame registration using edges, we compare the accuracy of registering edges from the segmented target shape with the accuracy of registering an entire 128x128 window. Both of these are registered against the 128x128 window of the next image. Twenty-five edges were used for target registration and ninety-seven were used in the window registration. If the registration results are approximately the same, then successive registration over the approximate target location and target size can be used for close-in aimpoint selection and homing. Registration accuracy is inversely proportional to the square root of the number of matching edges. Hence, a

larger number of edges are found in the 128x128 window, and registration between windows will be more accurate. This will be the standard for comparison.

However, at close range, the density of repeatable edges over the target should be higher; hence, successive registrations should be fairly accurate also. The images for the example are taken from the NV&EOL 875-line FLIR data base described in the First Quarterly, Section 2.2.5 "Tape 5 11/14/77", Tape Position 5060. The helicopter is closing on a tank moving along a narrow road; the helicopter approaches the tank from the rear. The thinned gradient output produced by the Westinghouse AUTO-Q System, described in Appendix A of the First Quarterly, is shown in Figure 4.2-10 for image 1784. The gradient directions are quantized at 45^0 increments as shown in Figure 4.2-9 which also shows the encoding for the computer output. The circular area is the hot engine of the moving tank as seen from the rear. Above the engine, one can see gradients representing structural features of the top and forward portions of the tank. The two vertical lines drawn in by pencil represent the edges of the narrow road upon which the tank is travelling. Figures 4.2-11 through 4.2-15 show the thinned gradient display

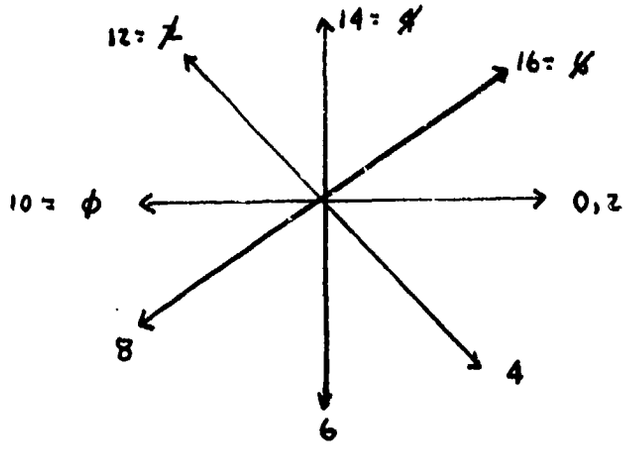

Figure 4.2-9. Gradient Directions

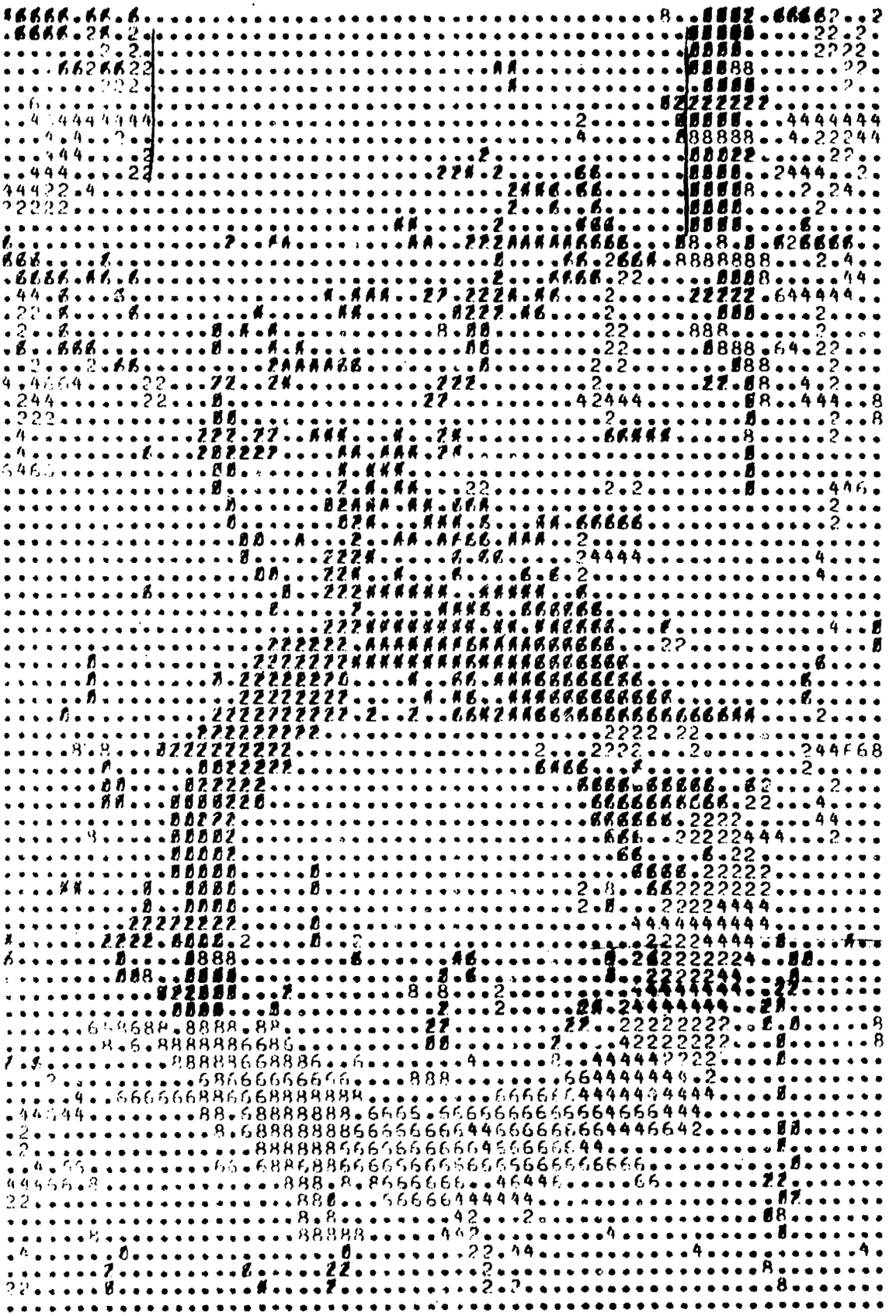

Figure 4.2-10. Thinned Gradient Direction Display, Image 1784

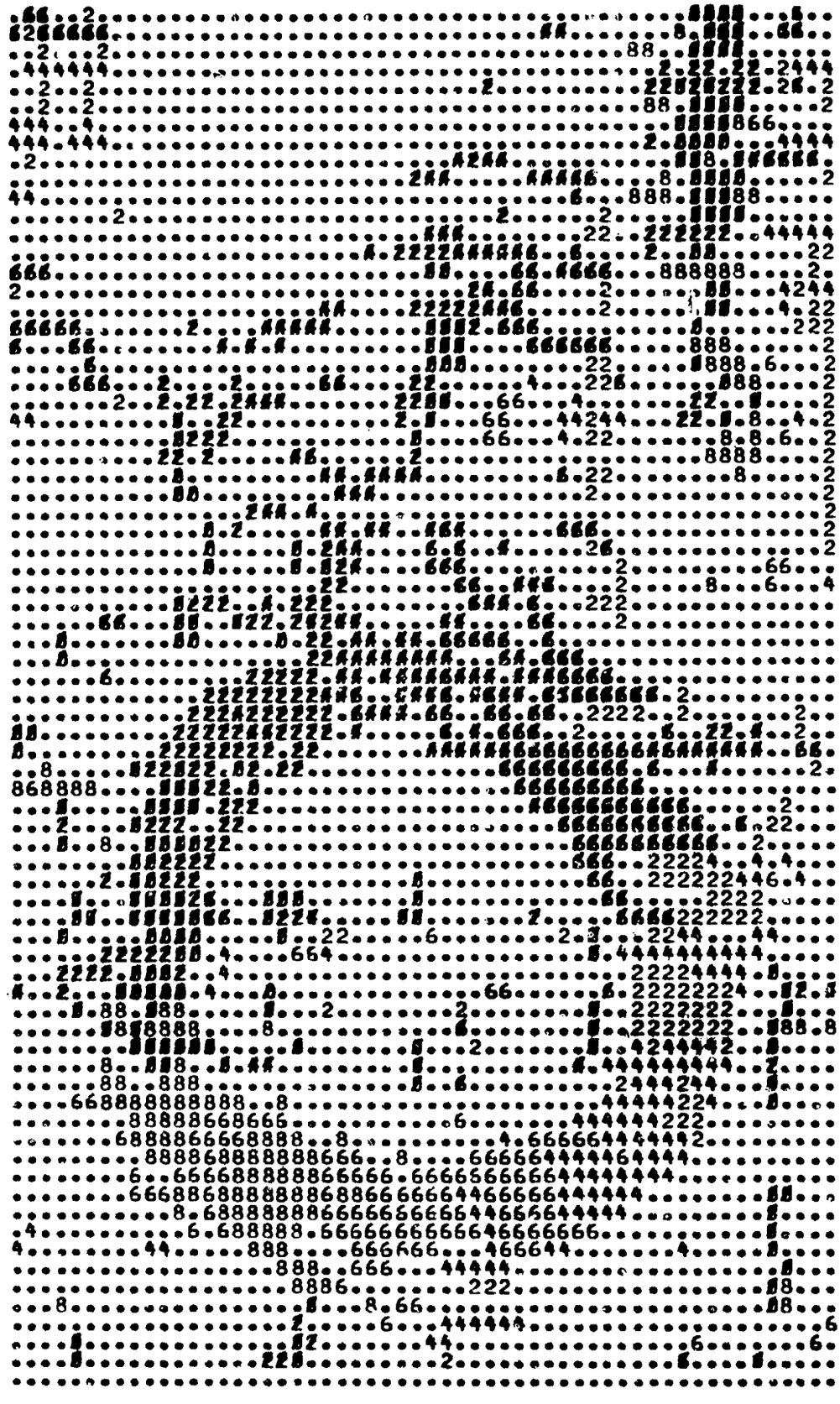

Figure 4.2-11. Thinned Gradient Direction Display, Image 1788

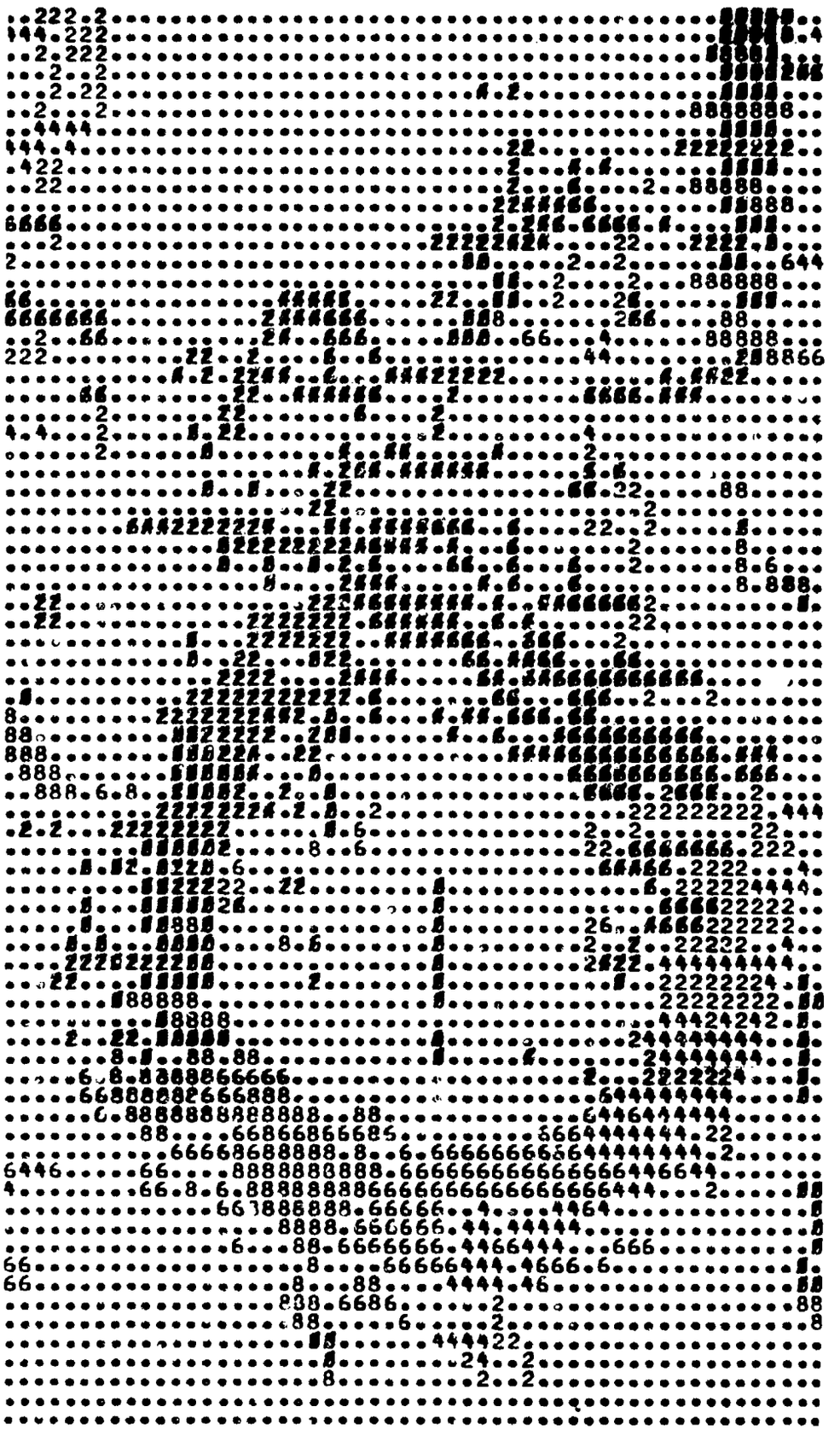

Figure 4.2-12. Thinned Gradient Direction Display, Image 1792

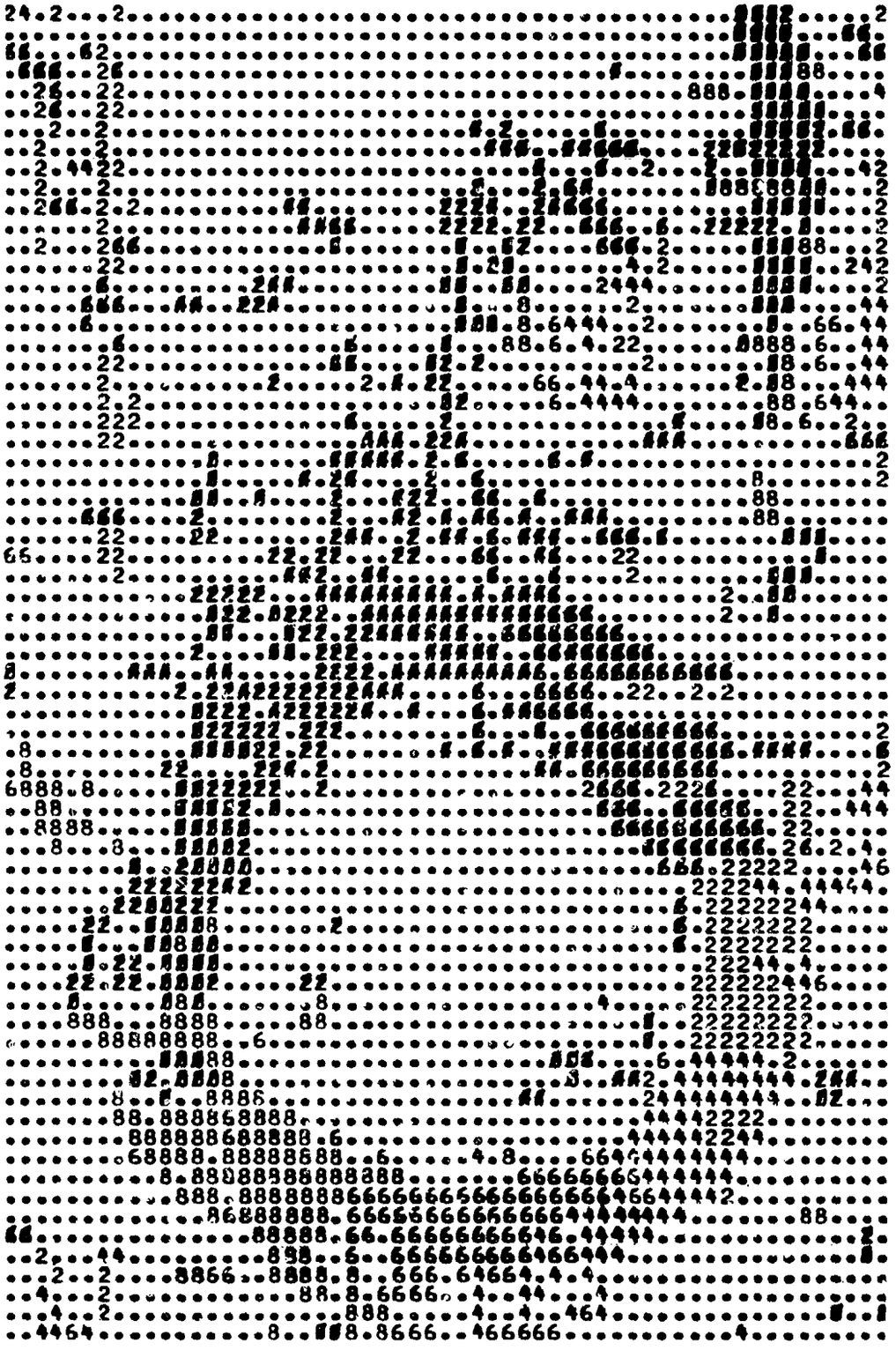

Figure 4.2-13. Thinned Gradient Direction Display, Image 1790

Figure 4.2-14. Thinned Gradient Direction Display, Image 1800

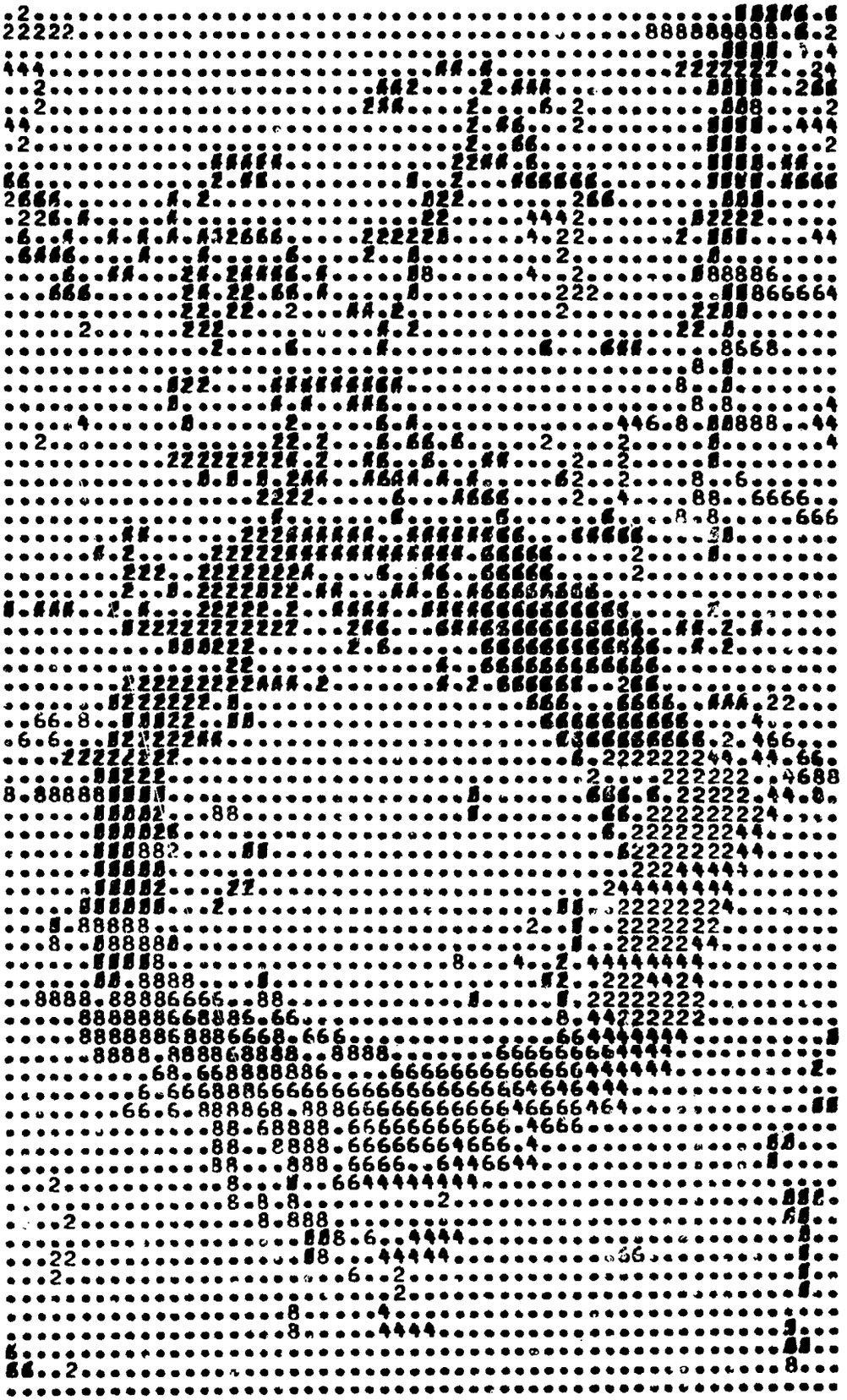

Figure 4.2-15. Thinned Gradient Direction Display, Image 1804

for images 1788, 1792, 1976, 1800, and 1804. The process for obtaining edges from the thinned gradient data is described in Appendix A of the first Quarterly Report in the section on the Westinghouse AUTO-Q System; the edges derived from images 1784, 1788, and 1792 are shown in Figures 4.2-16 through 4.2-18. Refer to Appendix A for a description of the registration process, the results of which are shown in Figure 4.2-19. The DELX and DELY are the offsets, rounded to the nearest pixel, between the present window and the proceeding one based on the registration results. The Full Window represents a 128x128 window containing the target registered against another 128x128 window containing the target. The Target Window represents a 60x50 window containing the target registered against a 128x128 window containing the target. The first two and the fourth result differ by one pixel; the third result is registered exactly, and the last result differs by 2.2 pixels.

In conclusion, it appears that on the whole, the notion of using frame-to-frame registration as a means of tracking close-in targets offers sufficient accuracy (one pixel) to be feasible and can be substantially speeded by using only a small window about the target. Such an approach may be necessary because of difficulties in 1) using correlation procedures in the presence of object contours, and 2) segmenting as one object a target which contains non-negligible interval contrasts and edges. Critical aimpoint selection procedures, in this case, would either depend on precise handoff and continued maintenance of the aimpoint derived by long range methods (with accuracy limited by resolution at the range of track mode transition) or on new methods employing the subsets which are yet to be developed.

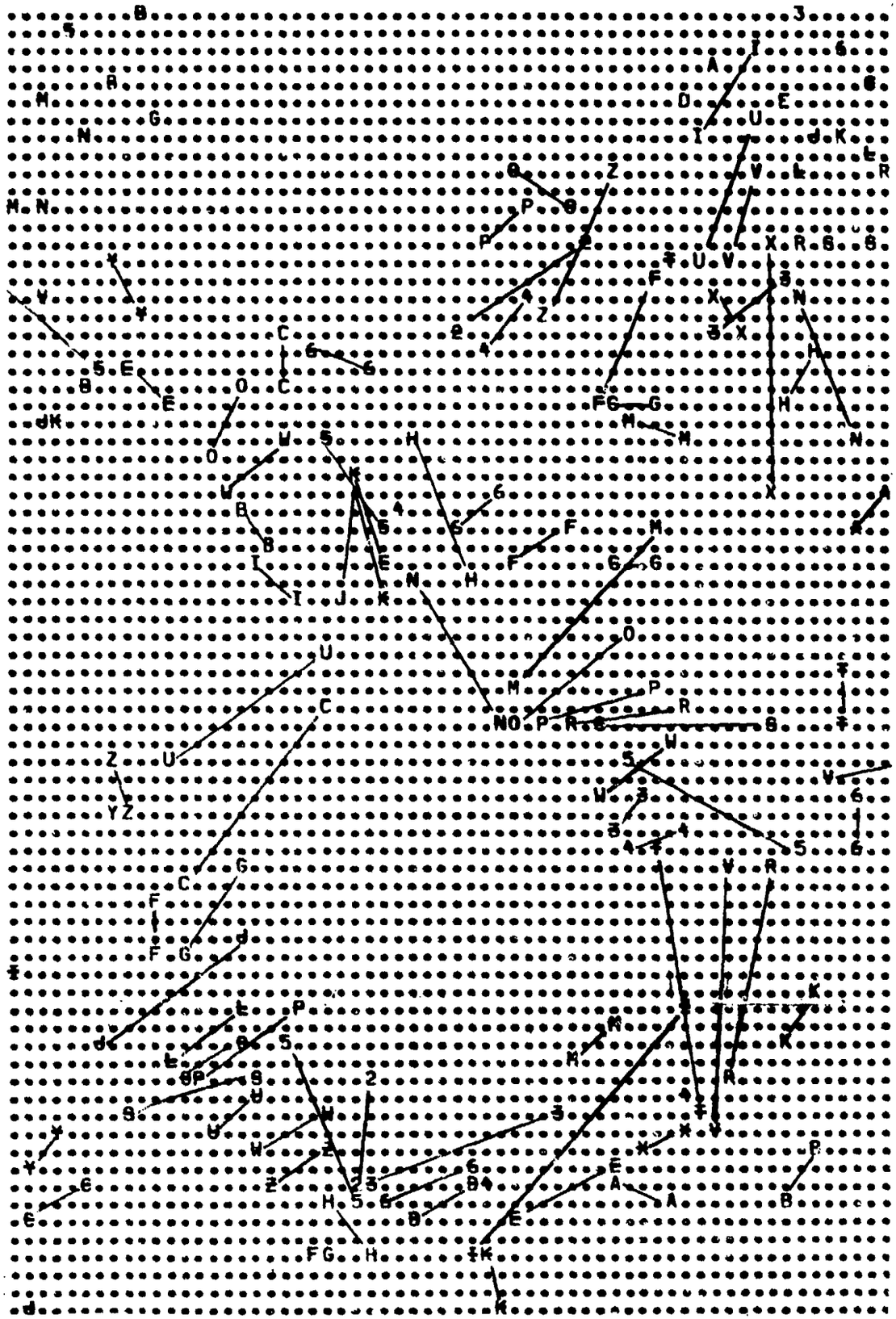

Figure 4.2-16. Subset/Blob Display, Image 1784

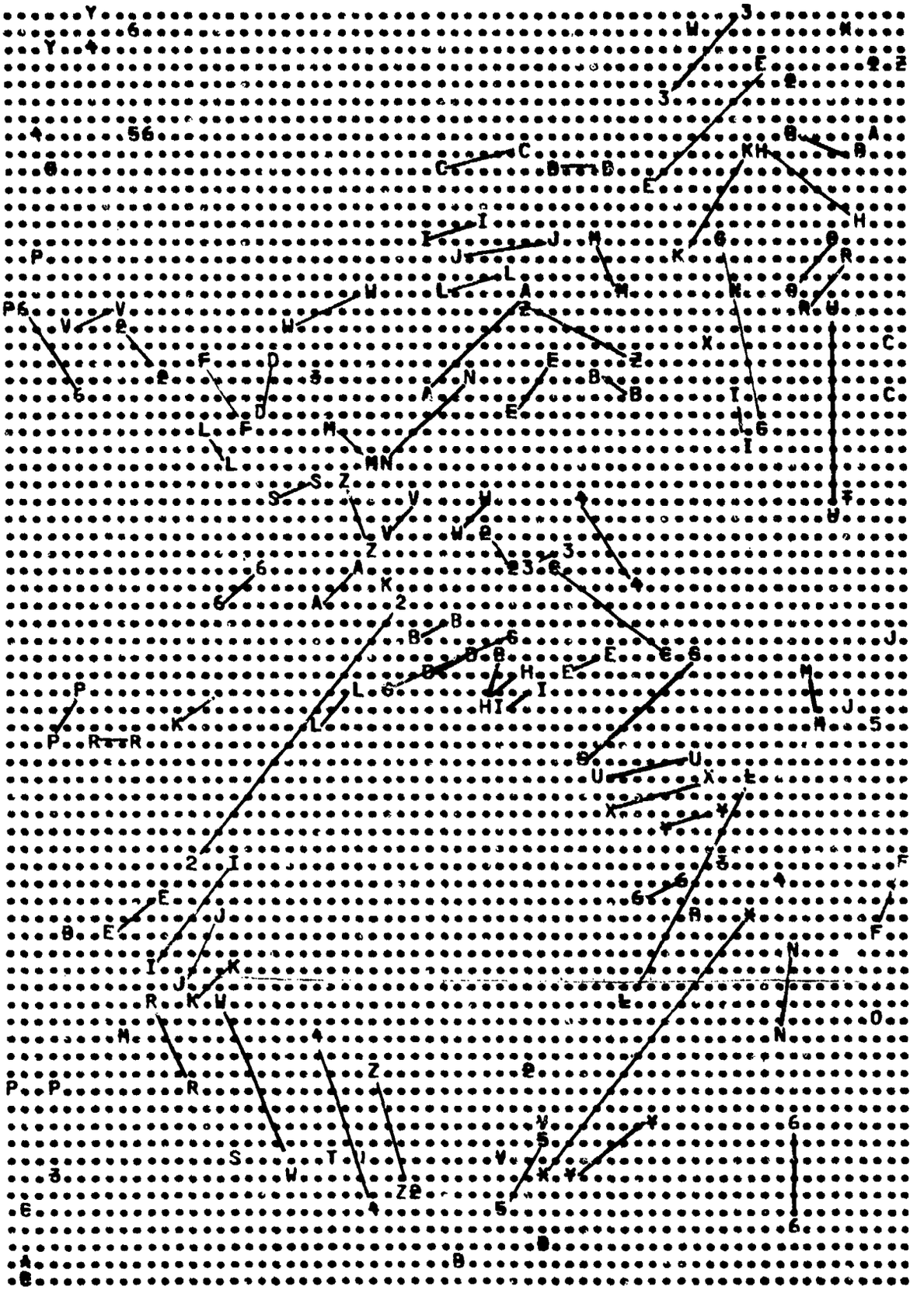

Figure 4.2-17. Subset/Blob Display, Image 1788

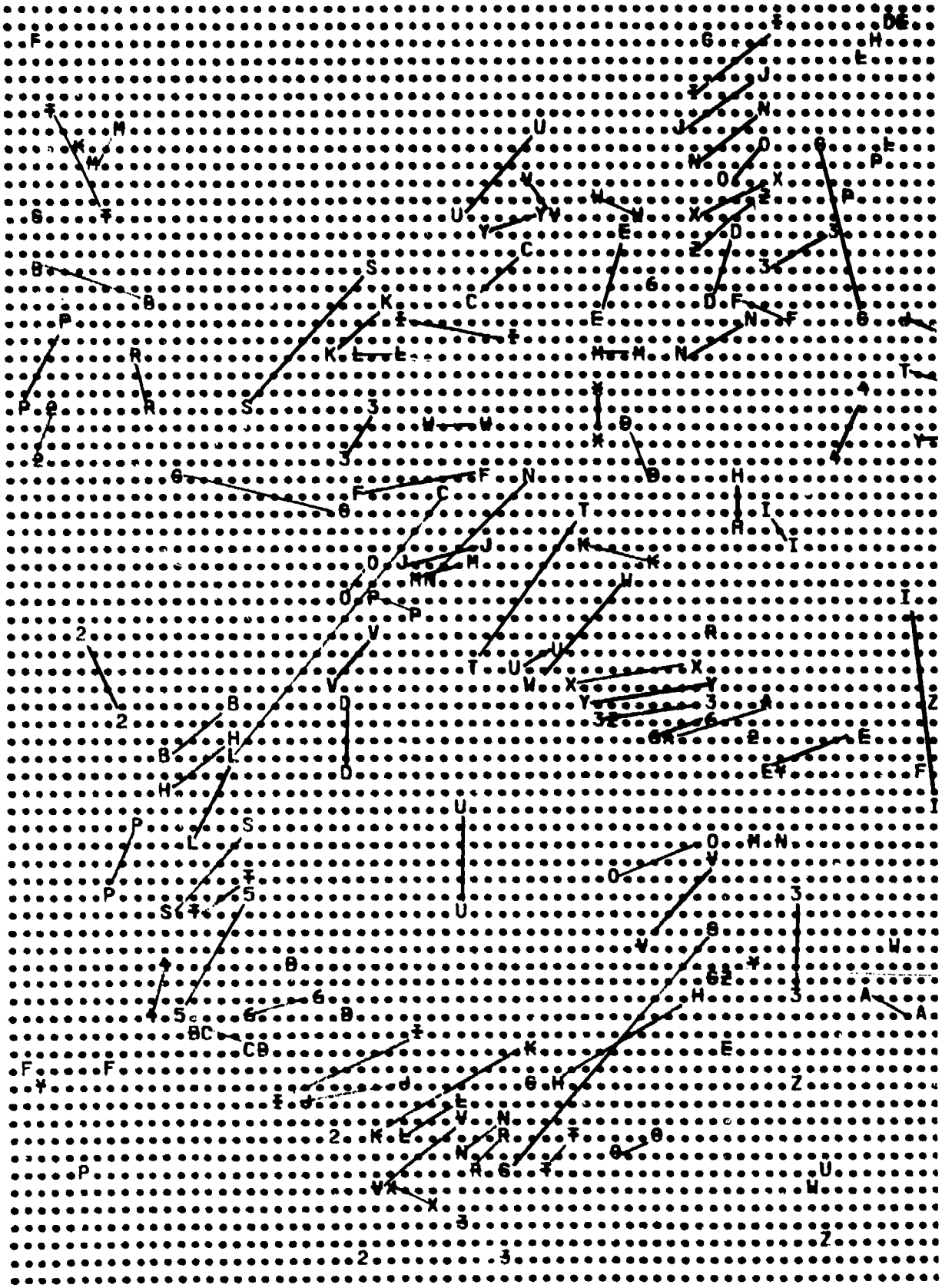

Figure 4.2-18. Subset/Blob Display, Image 1792

	FULL WINDOW		TARGET WINDOW	
	DELX	DELY	DELX	DELY
1788vs 1784	1	1	2	1
1792vs 1788	1	0	1	-1
1796vs 1792	1	-5	1	-5
1800vs 1796	3	4	2	4
1804vs 1800	1	2	-1	1

Figure 4.2-19. Comparison of Offsets (Pixels) for Succeeding Registrations

4.2.3 Tracking During Transition

The purpose of this section is to discuss tracking during the transition from long range aimpoint selection and homing to close-in aimpoint selection and homing. In Section 4.1, we presented a concept and examples of long range aimpoint selection; in Section 4.2.2, we presented a concept for close-in segmentation and an example. Here, we consider the transition from one to the other or "hand-over", if you will. There are two parts to the problem. One question is the accuracy of handing over from binary correlation tracking to edge tracking, another question is the accuracy of edge tracking itself. In general, edge tracking accuracy, which is really successive, frame-to-frame registration, is proportional to the initial offset between frames and inversely proportional to the square root of the number of edges used. To test edge tracking accuracy the following procedure is employed.

The Westinghouse lab equipment, at present, extracts a 128x128 pixel window from a video tape. Thus, the largest window for the successive registration test is 128x128 pixels. Within the 128x128 pixel window is the 30x30 pixel target. Since the registration accuracy is inversely proportional to the number of edges used, successive registrations of 128x128 windows can be more accurate than a 30x30 window registered against the following 128x128 window. In other words, the accuracy of registering the 30x30 target against the following 128x128 window can be evaluated by comparing it with the registration of the full 128x128 window, containing the 30x30 target, against the following 128x128 window. Since the same window pairs are used for each registration, the offset is the same for both registrations. The data for this example is from the NV&EOL 875 FLIR data set as described in the First Quarterly in Section 2.2.5. The video tape is "Tape #5 11/14/77", Tape Position 5280. It is a side view of a tank, moving from right to left across the field of view. To verify the

accuracy of the edge registrations the contents of the track window are registered against the 128x128 subsequent window. This result is compared against a registration of the entire 128x128 window against the following 128x128 window. If the point of maximum correlation occurs at the same x,y position for the 30x30 vs. 128x128 as the 128x128 vs. 128x128 for the same successive frames, the accuracy test is successful. Figure 4.2-20 shows the x,y coordinates for the point of maximum correlation for several sets of windows for both types of registration, i.e. 128x128 vs. 128x128 and 30x30 vs. 128x128. An examination of Figure 4.2-20 shows that the maximum correlation points for both types of registration differ by 0.5 pixels or less. Hence, the 30x30 pixel vs. 128x128 pixel registration offers sufficient accuracy. We shall discuss this result more in the conclusions to this section, but we want to develop another result first.

MAXIMUM CORRELATION POINTS (x,y)

WINDOWS REGISTERED	X		Y	
	128x128 vs. 128x126	30x30 vs. 128x128	128x128 vs. 128x128	30x30 vs. 128x128
408 vs. 404	10.33	10.20	12.83	12.40
412 vs. 408	9.48	9.10	11.80	11.26

Figure 4.2-20. Coordinates of Point of Maximum Correlation for both Types of Registration

Thus far, we have discussed the second problem associated with tracking during transition. We now discuss the first one; namely, the accuracy of handing over from binary correlation to edge tracking. Note, that in Figure 4.2-20, the target movement from frame-to-frame was not described. We merely talked in terms of the point of maximum correlation and never discussed the displacement of one image relative to the other to obtain a maximum correlation value. In comparing binary correlation tracking against edge tracking for the same, successive frames, this displacement is used to make the comparison. The aimpoint computations and frame-to-frame tracking results for images 404, 408, and 412 are shown in Figures 4.2-21, 4.2-22, and 4.2-23. Note that the movement of the track window within the image is included in the aimpoint computations also. Thus, $\Delta x = 2$, $\Delta y = 0$ from image 404 to 408 and $\Delta x = 4$, $\Delta y = 1$ from images 408 to 412. The Δx, Δy displacements indicate the relative displacement of the second track window, for image 408, from the first, image 404. Since the track window size is the same, Δx, Δy are equivalent to the relative displacement of the point of maximum correlation. In Figure 4.2-24, we show the relative displacements of the maximum correlation points for both sets of images. Also included are the relative displacements of the points of maximum correlation for the 30x30 vs. 128x128 and 128x128 vs. 128x128 edge registration approaches, rounded to the nearest pixel.

Note that the error in displacement between the binary correlation tracker and the 30x30 vs. 128x128 edge tracking is

$$\sqrt{(\Delta x_1 - \Delta x_2)^2 + (\Delta y_1 - \Delta y_2)} = \sqrt{2} \quad ;$$

in both cases, this is a measure of the accuracy of the handover process. In the binary correlation against 128x128 edge tracking, the error is 1.0 pixels and 1.4 pixels, respectively. By the standards of registration for large windows (500x500) where the registration accuracy can approach 0.25 pixels, this result is not impressive. However, the 1.4 pixel error in placing the 32x32 track window is not very serious and appears to be adequate.

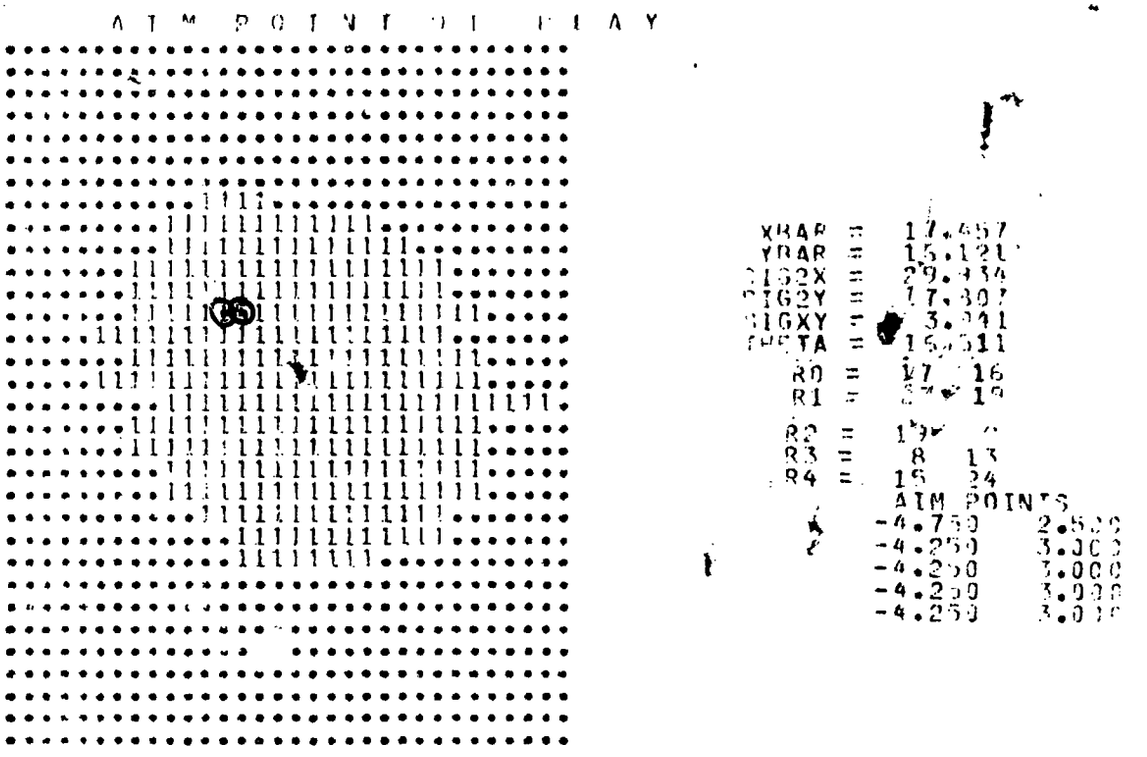

Figure 4.2-21. Aimpoint Computations, Image 404

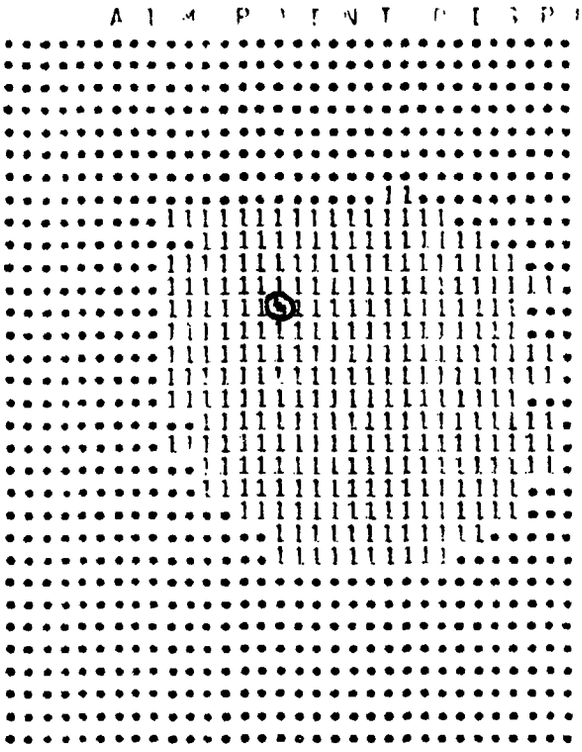

DELX = 2 DELY =
DIRC = 0
XBAR = 20.258
YBAR = 16.074
SIG2X = 32.084
SIG2Y = 18.471
SIGXY = 2.971
THETA = -11.759
R0 = 20 13
R1 = 31 18
R2 = 22 8
R3 = 10 14
R4 = 19 24
AIM POINTS
-4.750 2.667
-4.750 2.667
-4.750 2.667
-4.750 2.667
-4.750 2.667

Figure 4.2-22. Aimpoint Computations, Image 408

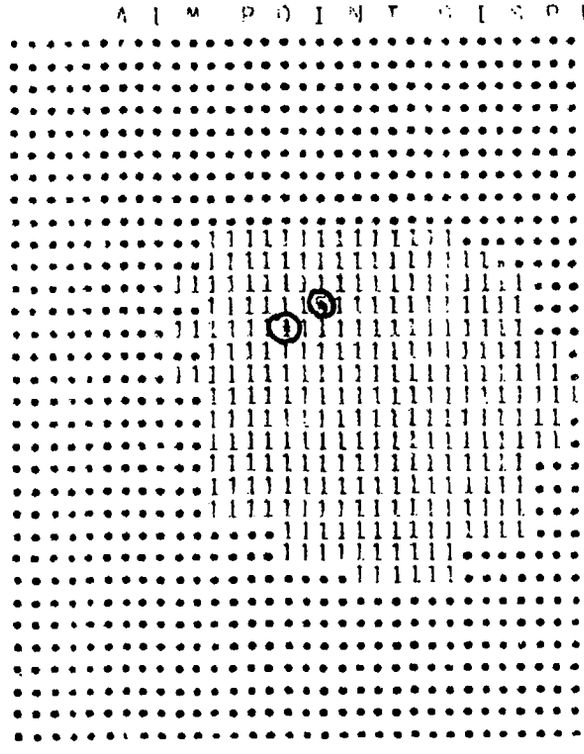

DELX = 4 DELY = 1
DIRC = 14
XBAR = 20.673
YBAR = 16.954
SIG2X = 24.471
SIG2Y = 17.125
SIGXY = 2.[illegible]
THETA = -11.[illegible]
R0 = 20 13
R1 = 31 18
R2 = 22 10
R3 = 12 15
R4 = 19 24
AIM POINTS
-4.750 3.[illegible]
-3.250 3.[illegible]
-3.250 3.[illegible]
-3.250 3.[illegible]
-3.250 3.[illegible]

Figure 4.2-23. Aimpoint Computations, Image 412

DISPLACEMENT OF MAXIMUM CORRELATION POSITIONS

	Δx			Δy		
WINDOWS COMPARED	Binary Correlation	30x30 vs. 128x128	128x128 vs. 128x128	Binary Correlation	30x30 vs. 128x128	128x128 vs. 128x128
408 vs. 404	2	1	1	0	1	0
412 vs. 408	4	5	5	1	2	2

Figure 4.2-24. Comparison of Correlation Displacement for Several Registration Approaches

In conclusion, these error magnitudes mean that the approximate target size and position from a previously cued or tracked window can be used to extract a window of gray code from the frame store (Section 1.0). The edges (subsets) can be extracted from this window and used to register against the entire image of the following frame with satisfactory accuracy. Hence, the handover to close-in homing and aimpoint selection can be accomplished because the aimpoint can be accurately placed, within 1.4 pixels, on the following image also.